Theoretical Study of Aqueous *N*-Acetyl-L-alanine *N*′-Methylamide: Structures and Raman, VCD, and ROA Spectra

Wen-Ge Han, K. J. Jalkanen, Marcus Elstner, and Sándor Suhai*

Department of Molecular Biophysics, German Cancer Research Center, Im Neuenheimer Feld 280, D-69120 Heidelberg, Germany

Received: July 15, 1997; In Final Form: January 22, 1998

Starting from the eight B3LYP/6-31G* optimized *N*-acetyl-L-alanine *N*′-methylamide (AAMA) structures recently reported by Jalkanen and Suhai,[1] we studied the effect of hydration on the AAMA geometries, relative energies, and vibrational properties by applying the solvent continuum model, by adding four explicit water molecules to each of the conformers, and finally by combining the two approaches. For the four lowest energy AAMA+4H_2O complexes, we have calculated the B3LYP/6-31G* Hessians and atomic polar tensors (APT), RHF/6-31G* atomic axial tensors (AAT), RHF/6-311+G** electric dipole−electric dipole polarizability derivatives (EDEDPD), RHF/6-31G* electric dipole−magnetic dipole polarizability derivatives (EDMDPD), and RHF/6-31G* electric dipole−electric quadrupole polarizability derivatives (EDEQPD), which gave us the required quantities to simulate the vibrational absorption (VA), Raman, vibrational circular dichroism (VCD), and Raman optical activity (ROA) spectra. The explicit water model reveals the H-bonding between the AAMA and the water molecules. The water stabilizes two AAMA structures (P_{II} and α_R), which are not stable in the isolated state. The influence of the explicit water molecules on the AAMA vibrational spectra was also discussed. The solvent continuum model applied to the AAMA+4H_2O complexes further modified the orientations of the water molecules and influenced the vibrational modes and intensities. By comparing the calculated and the observed Raman, VCD, and ROA spectra, we suggest that the P_{II} structure of AAMA ($\phi \sim -93°$, $\psi \sim 128°$) is the dominant one in aqueous solutions.

1. Introduction

In a recent paper[1] we have calculated the vibrational absorption (VA) and vibrational circular dichroism (VCD) spectra of eight conformers of AAMA in the isolated state and one of its conformers in the presence of four water molecules. The VA and VCD spectra were compared to the measured VA and VCD spectra of AAMA isolated in low-temperature Ar matrixes and dissolved in inert solvents. Here we will analyze the experimental Raman, VCD, and Raman optical activity (ROA) spectra of AAMA in aqueous solutions.

AAMA has been extensively studied as one of the primary models of the protein backbone. Two major degrees of freedom determine its conformation: ϕ ($C_1-N_2-C_4-C_{10}$) and ψ ($N_{16}-C_{10}-C_4-N_2$) (see Figure 1a). The experimental VA spectra[2] have shown and theoretical calculations[1,3−9] have confirmed that the C_7^{eq} ($\phi \sim -80°$, $\psi \sim 70°$) and C_5^{ext} ($\phi \sim -160°$, $\psi \sim 170°$) conformers of AAMA are of the dominant species present at room temperature in CCl_4 solution and at low temperature in Ar matrixes.

The VA and VCD spectra of CD_3CN, H_2O, and D_2O solutions of AAMA in the amide I and III regions have been measured by the M. Diem group in New York.[10,11] They found that the VCD spectra were very sensitive to the solvent type, the solute concentration, and the temperature. The cause of the spectral changes is not yet fully understood. It may be due to the changes in intermolecular association as a function of the AAMA concentration or due to changes in conformations of the AAMA as concentration, temperature, and solvent are varied. The Raman spectra of the AAMA in aqueous solutions were measured by Avignon et al.[12] Very recently, Deng et al. reported both the experimental Raman and ROA spectra of $CHCl_3$, H_2O, and D_2O solutions of AAMA.[13] They also predicted the Raman and ROA spectra of nine conformations of AAMA at the RHF/6-31G*/6-31G level of theory. They did not include, however, any solvent effects in their calculations. Their basis set, 6-31G, for the polarizability derivative tensors did not include any polarization functions. Here we use the 6-311+G** basis set for the EDEDPD and use the 6-31G* basis set for the EDMDPD and EDEQPD calculations. We extend the previous studies in that we use the B3LYP level of theory, which includes electron correlation, and we also include water molecules, both explicitly and implicitly, in calculating the structures and APT. Previous work on the Raman and ROA spectra have been at the RHF level of theory for the geometry and force field as well as for the polarizability tensors, and the solvent effect (water) was not taken into account.

There are two main methods to predict the solvation effect on properties of the solutes. The first one is to explicitly include the solvent molecules, using ab initio calculations or simulation methods (molecular dynamics, Monte Carlo, etc.) employing classical force fields. The second one is to use the reaction field continuum models where explicit solvent molecules are not considered.[14]

In the case of the H_2O solution, the explicit solvation model can reveal detailed information about the H-bonding between the solute and water molecules. The solute and its H-bonded water molecules are actually vibrationally coupled.[15,16] For

* Corresponding author.

S1089-5647(97)02299-2 CCC: $15.00
Published on Web 03/13/1998

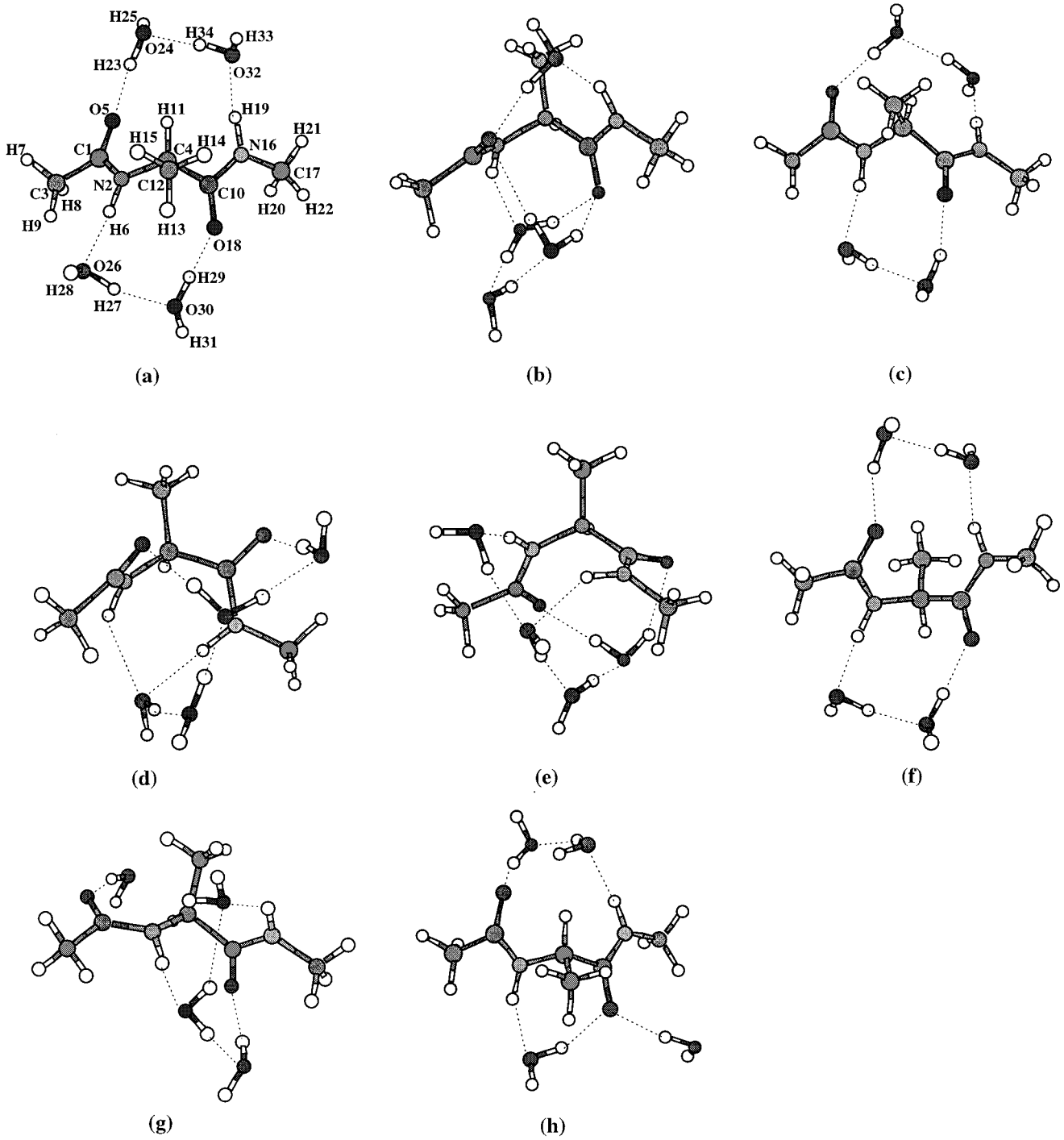

Figure 1. Eight optimized AAMA+4H_2O conformers: (a) P_{II}, (b) $C_7^{ax'}$, (c) β_2', (d) α_L', (e) α_R', (f) α_D', (g) α_P', (h) Crystal.

higher level (ab initio) calculations, however, it is not possible to treat the bulk solvent molecules explicitly. On the other hand, the reaction field solvent continuum models may predict the effect of the bulk water but cannot give detailed information about H-bonding.

For studying the solvation effect on the conformational distribution of AAMA, many calculations such as Monte Carlo simulations, molecular dynamics/mechanics simulations, and the extended RISM integral equation method have been performed by solvating the AAMA with explicit water molecules or using the continuum solvation model.[7,9,13,17−23] Most of these studies show that the P_{II} ($\phi = -110°$ to $-70°$, $\psi = 120°$ to $150°$) and the α_R ($\phi = -90°$ to $-60°$, $\psi = -60°$ to $-40°$) conformers of AAMA are stabilized due to the hydration effect. However, the solvent corrections and energy calculations are dependent on the type of model used to incorporate the solvent effect and the level of theory used in the calculations.

So far, not much effort has been made to predict the VCD, Raman, and ROA spectra of AAMA in aqueous solution. Our previous studies[1,24] have documented the possibility of including H-bonded water in density functional theory (DFT)[25,26] calculations and in simulating the VA and VCD spectra of small peptides.

Here we have investigated the effects of the various ways to model the solvent (simple continuum treatment, explicit waters, and finally combining the two approaches) on the structure, energy, and VA, VCD, and Raman spectra of AAMA. The ROA spectra are only simulated at the highest level of theory

and are used to help answer the question: which conformer(s) of AAMA are present in aqueous solution?

In section 2, we describe our models and methods for the spectral calculations. In section 3, we present and discuss the effects of different solvation methods on the structures and energies of the AAMA conformers and the influence of the explicit water molecules on AAMA vibrational spectra. We also present our predicted Raman, VCD, and ROA spectra and compare them with the experimental results. In section 4 we present our conclusions.

2. Methods

2.1. Determination of Structures. Our study of AAMA is based on the eight 6-31G* B3LYP optimized isolated AAMA structures reported by Jalkanen and Suhai.[1] To see the hydration effect on AAMA using the self-consistent reaction field (SCRF) methods, we have reoptimized the eight structures using the Onsager and SCIPCM models as implemented in Gaussian 94.[27] We used $\epsilon = 80.0$ as the dielectric constant of water.

To see the details of the H-bonding between the AAMA conformers and the water molecules, we solvated each of the eight AAMA conformers with four water molecules by using the program INSIGHT/DISCOVER.[32] According to the studies of Beglov and Roux,[33] four water molecules can be considered as the primary hydration shell of AAMA. Firstly, we soaked the molecule with two layers of water (about nine water molecules) and then fixed the backbone structure and only optimized the positions of the water molecules using the CFF91 force field and the VA09A minimizer to the convergence criterion of 0.01 kcal mol^{-1} Å^{-1}. Sometimes we needed to repeat this step several times until each of the C═O and N−H bonds had at least one hydrogen bond formed with water molecules. We kept the four water molecules which formed H-bonds with AAMA and deleted the others. Then again the backbone angles were frozen and the four water positions were optimized to a convergence criterion of 0.001 kcal mol^{-1} Å^{-1}. Finally the full geometry was optimized using the CFF91 force field but with the Newton−Raphson minimizer to the convergence criterion of 0.000 001 kcal mol^{-1} Å^{-1}. Afterward, the eight solvated conformers were optimized at the (G94) B3LYP/6-31G* level.

Five models were used in this paper: (1) AAMA in isolated state, (2) AAMA within the Onsager model, (3) AAMA within the SCIPCM model, (4) AAMA+4H_2O, and (5) AAMA+4H_2O within the Onsager model.

2.2. Spectral Calculations. For the four lowest energy optimized structures in models 4 and 5, we have calculated the Hessians and atomic polar tensors (APT) at the (G94) B3LYP/6-31G* level. For calculating the VCD, Raman and ROA spectra, one has to have atomic axial tensors (AAT), electric dipole−electric dipole polarizability derivatives (EDEDPD), electric dipole−magnetic dipole polarizability derivatives (EDMDPD), and electric dipole−electric quadrupole polarizability derivatives (EDEQPD). The publicly released versions of G94 have no capability to calculate the AAT and EDEDPD at the DFT level. We have therefore used G94 to calculate the RHF/6-311+G** level EDEDPD and used CADPAC[34] to calculate the RHF/6-31G* level AAT. By combining the tensors and Hessians, we obtained the VA, Raman, and VCD spectra for these structures. For the ROA spectra we also require the EDMDPD and EDEQPD. These tensor derivatives have not been implemented to date in any program, but the tensors themselves have been implemented in CADPAC by R. D. Amos.[35]

We use CADPAC to calculate the electric dipole−magnetic dipole polarizabilities (EDMDP) and electric dipole−electric quadrupole polarizabilities (EDEQP) at displaced geometries to calculate the polarizability derivatives numerically. Note that Bak and co-workers in Denmark have recently implemented the equations to calculate the EDMDP and EDEQP tensors in their suite of ab initio programs called DALTON.[36] Note that by using London atomic orbitals they treat the problem of gauge dependence of the EDMDP and EDMDPD more rigorously than did previous attempts to simulate the ROA spectra.[37] Their calculations using the London atomic orbitals at the RHF/6-31G* level of theory were very similar to the RHF/6-31G* calculations using conventional atomic orbitals in CADPAC. Hence we are confident in utilizing this level of theory but also realize that the calculations could be improved by performing the calculations using London atomic orbitals.

With a variety of basis sets, Bak and co-workers calculated the RHF EDMDPD and EDEQPD and combined them with the RHF Hessian to predict the ROA spectra for methyloxirane.[36] Here they found that, even at the Hartree−Fock limit, four sign differences between the calculated and experimental ROA spectra were present. Since one should not expect to predict all of the signs for the ROA spectra using Hartree−Fock limiting basis sets, we must be careful here in analyzing our comparison to the experimental ROA spectra for AAMA in aqueous solution. Here we may also be able to determine which modes the current theory is able to predict accurately in the ROA spectra.

2.2.1. VA and VCD Calculations. The methodology of obtaining the VA and VCD intensities from the Hessians, APT, and AAT was given in ref 1.

2.2.2. Raman and ROA Calculations. When one wishes to calculate the Raman and ROA spectra, one needs the derivatives of the EDEDP, the EDMDP, and the EDEQP as well as the frequencies and normal modes which one can get from the Cartesian or internal cooordinate Hessian (second derivatives of the energy with respect to nuclear displacements of each atom). The analytical calculation of the EDEDPD has been implemented at the RHF level in CADPAC[38] and also in Gaussian 94.[39] We used both CADPAC and Gaussian 94 to calculate all of these tensor derivatives.

The EDEDPD can be calculated as the third derivative of the energy (W_G) with respect to two electric fields (E) and the nuclear displacement, that is,

$$\alpha_{\beta\gamma}^{\lambda\alpha} = \left(\frac{\partial^3 W_G(\vec{R}, E_\beta, E_\gamma)}{\partial X_{\lambda\alpha}\, \partial E_\beta\, \partial E_\gamma}\right)_{\vec{R}=\vec{R}_0, E_\beta=0, E_\gamma=0} = \left(\frac{\partial \alpha_{\beta\gamma}(\vec{R})}{\partial X_{\lambda\alpha}}\right)_{\vec{R}=\vec{R}_0} \quad (1)$$

$\alpha, \beta, \gamma = x, y,$ or z, λ specifies a nucleus, and X is the Cartesian displacement coordinate.

We know that the Raman intensity is proportional to the Raman scattering activity, and the Raman scattering activity of the jth normal mode Q_j is given by

$$I_j^{\mathrm{Ram}} = g_j(45\bar{\alpha}_j^{\,2} + 7\bar{\beta}_j^{\,2}) \quad (2)$$

where g_j is the degeneracy of the jth transition. If we present $\sum_{\lambda\alpha} S_{\lambda\alpha,j}\alpha_{\delta\gamma}^{\lambda\alpha}$ just as $S_{\lambda\alpha,j}\alpha_{\delta\gamma}^{\lambda\alpha}$ ($\delta, \gamma = x, y,$ or z), then $\bar{\alpha}_j$ (the mean polarizability derivative tensor) and $\bar{\beta}_j^2$ (the anisotropy of the polarizability tensor derivative) are given by

$$\bar{\alpha}_j^2 = \frac{1}{9}(S_{\lambda\alpha,j}\alpha_{xx}^{\lambda\alpha} + S_{\lambda\alpha,j}\alpha_{yy}^{\lambda\alpha} + S_{\lambda\alpha,j}\alpha_{zz}^{\lambda\alpha})^2 \quad (3)$$

$$\bar{\beta}_j^2 = \frac{1}{2}\{(S_{\lambda\alpha,j}\alpha_{xx}^{\lambda\alpha} - S_{\lambda\alpha,j}\alpha_{yy}^{\lambda\alpha})^2 + (S_{\lambda\alpha,j}\alpha_{xx}^{\lambda\alpha} - S_{\lambda\alpha,j}\alpha_{zz}^{\lambda\alpha})^2 + (S_{\lambda\alpha,j}\alpha_{yy}^{\lambda\alpha} - S_{\lambda\alpha,j}\alpha_{zz}^{\lambda\alpha})^2 + 6[(S_{\lambda\alpha,j}\alpha_{xy}^{\lambda\alpha})^2 + (S_{\lambda\alpha,j}\alpha_{yz}^{\lambda\alpha})^2 + (S_{\lambda\alpha,j}\alpha_{xz}^{\lambda\alpha})^2]\} \quad (4)$$

where the $S_{\lambda\alpha,j}$ matrix relates the normal coordinates Q_j to Cartesian displacement coordinates $X_{\lambda\alpha}$ and again λ specifies a nucleus and $\alpha = x$, y, or z.[40]

$$X_{\lambda\alpha} = \sum_i S_{\lambda\alpha,i}Q_i \quad (5)$$

We know that the normal frequencies are the eigenvalues Λ of the Hessian matrix H:

$$C^{-1}HC = \Lambda \quad (6)$$

C is the eigenvector matrix, which defines the transformation matrix S:

$$S = M^{-1/2}C \quad (7)$$

where M is the mass matrix.

Therefore, through the matrix S (obtained by diagonalizing the Hessian matrix) and the EDEDPD $\alpha_{\delta\gamma}^{\lambda\alpha}$, one can obtain the Raman scattering activity of any normal mode Q_j.

The ROA calculation, in addition to requiring the EDEDPD, requires the EDMDPD and the EDEQPD. The EDMDP, G', can be evaluated as the second derivative of the energy with respect to a static electric field and a time-varying magnetic field. Hence the EDMDPD is a third derivative, with the third derivative being with respect to the nuclear displacement.

$$G'^{\lambda\alpha}_{\beta\gamma} = \left(\frac{\partial^3 W_G(\vec{R},F_\beta,\dot{B}_\gamma)}{\partial X_{\lambda\alpha}\,\partial F_\beta\,\partial\dot{B}\gamma}\right)_{\vec{R}=\vec{R}_0,F_\beta=0,\dot{B}_\gamma=0} = \left(\frac{\partial G'_{\beta\gamma}(\vec{R})}{\partial X_{\lambda\alpha}}\right)_{\vec{R}=\vec{R}_0} \quad (8)$$

The EDEQP, A, can be evaluated as the second derivative of the energy with respect to a static electric field and a static electric field gradient. Hence the EDEQPD is a third derivative, again the third derivative with respect to the nuclear displacement.

$$A_{\beta,\gamma\delta}^{\lambda\alpha} = \left(\frac{\partial^3 W_G(\vec{R},F_\beta,F'_{\gamma\delta})}{\partial X_{\lambda\alpha}\,\partial F_\beta\,\partial F'_{\gamma\delta}}\right)_{\vec{R}=\vec{R}_0,F_\beta=0,F'_{\gamma\delta}=0}\left(\frac{\partial A_{\beta,\gamma\delta}(\vec{R})}{\partial X_{\lambda\alpha}}\right)_{\vec{R}=\vec{R}_0} \quad (9)$$

These Cartesian polarizability derivatives are required to calculate the ROA spectra. The quantities required have been derived by Barron and Buckingham[41] and are γ_j^2 and δ_j^2.[42−44] They are calculated by combining the various polarizability derivatives with the normal mode vectors in the following equations:

$$\gamma_j^2 = \frac{1}{2}\{(S_{\lambda\alpha,j}\alpha_{xx}^{\lambda\alpha} - S_{\lambda\alpha,j}\alpha_{yy}^{\lambda\alpha})(S_{\lambda\alpha,j}G'^{\lambda\alpha}_{xx} - S_{\lambda\alpha,j}G'^{\lambda\alpha}_{yy}) + (S_{\lambda\alpha,j}\alpha_{xx}^{\lambda\alpha} - S_{\lambda\alpha,j}\alpha_{zz}^{\lambda\alpha})(S_{\lambda\alpha,j}G'^{\lambda\alpha}_{xx} - S_{\lambda\alpha,j}G'^{\lambda\alpha}_{zz}) + (S_{\lambda\alpha,j}\alpha_{yy}^{\lambda\alpha} - S_{\lambda\alpha,j}\alpha_{zz}^{\lambda\alpha})(S_{\lambda\alpha,j}G'^{\lambda\alpha}_{yy} - S_{\lambda\alpha,j}G'^{\lambda\alpha}_{zz}) + 3[(S_{\lambda\alpha,j}\alpha_{xy}^{\lambda\alpha})(S_{\lambda\alpha,j}G'^{\lambda\alpha}_{xy} + S_{\lambda\alpha,j}G'^{\lambda\alpha}_{yx}) + (S_{\lambda\alpha,j}\alpha_{yz}^{\lambda\alpha})(S_{\lambda\alpha,j}G'^{\lambda\alpha}_{yz} + S_{\lambda\alpha,j}G'^{\lambda\alpha}_{zy}) + (S_{\lambda\alpha,j}\alpha_{xz}^{\lambda\alpha})(S_{\lambda\alpha,j}G'^{\lambda\alpha}_{xz} + S_{\lambda\alpha,j}G'^{\lambda\alpha}_{zx})]\} \quad (10)$$

and δ_j^2 is given by

$$\delta_j^2 = \frac{\omega}{2}\{(S_{\lambda\alpha,j}\alpha_{yy}^{\lambda\alpha} - S_{\lambda\alpha,j}\alpha_{xx}^{\lambda\alpha})S_{\lambda\alpha,j}A_{z,xy}^{\lambda\alpha} + (S_{\lambda\alpha,j}\alpha_{xx}^{\lambda\alpha} - S_{\lambda\alpha,j}\alpha_{zz}^{\lambda\alpha})S_{\lambda\alpha,j}A_{y,zx}^{\lambda\alpha} + (S_{\lambda\alpha,j}\alpha_{zz}^{\lambda\alpha} - S_{\lambda\alpha,j}\alpha_{yy}^{\lambda\alpha})S_{\lambda\alpha,j}A_{x,yz}^{\lambda\alpha} + S_{\lambda\alpha,j}\alpha_{xy}^{\lambda\alpha}(S_{\lambda\alpha,j}A_{y,yz}^{\lambda\alpha} - S_{\lambda\alpha,j}A_{z,yy}^{\lambda\alpha} + S_{\lambda\alpha,j}A_{z,xx}^{\lambda\alpha} - S_{\lambda\alpha,j}A_{x,xz}^{\lambda\alpha}) + S_{\lambda\alpha,j}\alpha_{xz}^{\lambda\alpha}(S_{\lambda\alpha,j}A_{y,zz}^{\lambda\alpha} - S_{\lambda\alpha,j}A_{z,zy}^{\lambda\alpha} + S_{\lambda\alpha,j}A_{x,xy}^{\lambda\alpha} - S_{\lambda\alpha,j}A_{y,xx}^{\lambda\alpha}) + S_{\lambda\alpha,j}\alpha_{yz}^{\lambda\alpha}(S_{\lambda\alpha,j}A_{z,zx}^{\lambda\alpha} - S_{\lambda\alpha,j}A_{x,zz}^{\lambda\alpha} + S_{\lambda\alpha,j}A_{x,yy}^{\lambda\alpha} - S_{\lambda\alpha,j}A_{y,yx}^{\lambda\alpha})\} \quad (11)$$

The equations relating these tensor derivatives to the ROA spectra are given by Barron.[42,45]

The commonly reported quantity reported from ROA measurements is the dimensionless quantity called the circular intensity differential (CID) defined as

$$\Delta_\alpha = \left(\frac{I_\alpha^R - I_\alpha^L}{I_\alpha^R + I_\alpha^L}\right) \quad (12)$$

where I_α^R and I_α^L are the scattered intensities with linear α-polarization in right- and left-circularly polarized incident light. The CID for backward scattering ROA can be expressed as[45]

$$\Delta(\text{backward}) = \left(\frac{24[\gamma_j^2 + \delta_j^2/3]}{c[45\bar{\alpha}^2 + 7\bar{\beta}^2]}\right) \quad (13)$$

where c is the speed of light.

Using these expressions, we can calculate the backscattered ROA spectra within the mechanical harmonic approximation.

We predicted the VA, VCD, and Raman spectra for four of our optimized AAMA+4H_2O complexes in both models 4 and 5. Furthermore, we applied ROA calculations on four AAMA conformers obtained from model 5. We will present and discuss our results in the following sections.

3. Results and Discussion

3.1. Comparison of the Geometries and the Relative Energies of the AAMA Conformers in Different Models. In Table 1 the ϕ, ψ angles and the relative energies, ΔE, of the eight AAMA structures calculated at the B3LYP/6-31G* level of theory for the five kinds of models are given. The results for the isolated AAMA molecule are taken from ref 1. The ϕ and ψ for the isolated state α_R structure were frozen at −60° and −40°, respectively. This isolated state structure of AAMA was not a stable point (a local minimum energy structure) on the B3LYP/6-31G* potential energy surface.

3.1.1. Isolated AAMA in the SCRF Models. When we reoptimized the geometries of the eight isolated state AAMA structures within the Onsager and SCIPCM models, respectively, the α_R and β_2 structures were not stable and moved to the same point (new structure), whose ϕ and ψ angles deviate from those of the isolated state β_2 structure by more than 10°. The structures of the other conformers in the solvent models do not change significantly from those for the isolated state. The intramolecular seven- and five-atom H-bonded C_7^{eq}, C_7^{ax}, and C_5^{ext} structures still exist. The SCRF RHF/6-31G** calculations of Gould et al.[9] also found that the α_R conformer collapsed to the β_2 conformer. The C_5^{ext} conformer could not be located, however, in their calculations. Due to solvent polarization, the C_1═O_5 and C_{10}═O_{18} bonds are lengthened in the two solvent

TABLE 1: Comparison of the ϕ and ψ (deg) and the Relative Energies ΔE (kcal/mol) of the Eight B3LYP/6-31G* Optimized AAMA Structures in Different Models

		C_7^{eq}	C_5^{ext}	β_2	C_7^{ax}	α_R	α_L	α_D	α_P
(1) AAMA[a]	ϕ	−81.91	−157.31	−135.86	73.77	−60.00	68.20	57.25	−169.36
	ψ	72.27	165.26	23.40	−60.02	−40.00	24.73	−133.45	−37.79
	ΔE	0.000	1.433	3.181	2.612	5.652	5.817	6.467	6.853
(2) AAMA in Onsager model	ϕ	−83.70	−160.40	−114.85	73.14	−113.91	66.61	56.70	−160.20
	ψ	66.96	167.78	5.70	−52.86	4.73	30.95	−134.88	−45.21
	ΔE	0.000	1.429	1.715	2.512	1.603	4.026	6.852	4.902
(3) AAMA in SCIPCM model	ϕ	−84.80	−156.91	−116.02	73.34	−115.51	61.99	54.26	−156.96
	ψ	70.51	158.99	11.03	−53.68	10.27	36.35	−136.13	−53.34
	ΔE	0.000	0.556	0.740	2.029	0.737	2.568	4.853	4.587
		P_{II}	Crystal	β_2'	$C_7^{ax'}$	α_R'	α_L'	α_D'	α_P'
(4) AAMA+4H_2O	ϕ	−93.55	−97.90	−150.88	58.88	−82.08	60.73	66.68	−152.94
	ψ	127.62	111.75	116.47	−121.92	−44.11	52.44	−111.27	−92.01
	ΔE	0.000	5.864	1.886	4.134	2.465	2.754	3.715	15.140
(5) AAMA+4H_2O in Onsager Model	ϕ	−92.74	−98.48	−151.95	58.61	−80.27	59.08	66.61	−117.74
	ψ	128.61	107.82	118.41	−122.46	−47.61	52.45	−111.10	−110.34
	ΔE	0.018	4.791	1.870	3.592	0.000	1.160	3.761	7.784

[a] Taken from ref 1, in which ϕ and ψ in α_R were frozen at −60° and −40°, respectively.

models, especially in the SCIPCM model. The average elongation of the C═O bonds is about 0.003 Å in the Onsager model and 0.008 Å within the SCIPCM model. Other bond lengths have no regular and significant changes.

In the first three models, i.e., when there are no explicit water molecules, the C_7^{eq} and C_5^{ext} conformers turn out to be the two most stable structures. In model 1, the energy of the C_7^{ax} conformer is lower than that of the β_2 conformer. But in the SCRF models 2 and 3, the β_2 and α_R conformers turn out to be more stable than the C_7^{ax} conformer. Within the SCIPCM model the energy differences between the C_7^{eq}, C_5^{ext}, β_2, and α_R conformers are very small. This supports many previous simulation results (see the review paper of Brooks and Case),[8] namely, that in water solution the low-energy portions of the AAMA potential energy surface become much broader.

The C_7^{eq} conformer is the most stable structure within the first three models, 1−3. Because of the intramolecular H-bonding between the C_1═O_5 and N_{16}−H_{19} groups in this conformer, the C_1═O_5 bonds are all longer than C_{10}═O_{18} bonds by about 0.007 Å. For the same reason, the N_{16}−H_{19} bond lengths are longer than those of N_2−H_6 on average by 0.008 Å; therefore, the amide A (N−H stretching) and amide I (C═O stretching) regions of the vibrational spectra of these dipeptide conformers should have split peaks. This is true for the Ar-matrix AAMA VA spectra obtained by Grenie et al.[2] This is evidence that, in the isolated state, the C_7^{eq} conformer AAMA is present.[1] Unfortunately, we have no experimental spectral data of the amide A region for AAMA in aqueous solutions. The experimental Raman spectra[12,13] of AAMA in H_2O and in D_2O solutions show that there is only one peak in the amide I region (1650 cm^{-1} in ref 12 or 1654 cm^{-1} in ref 13 in H_2O and 1632 cm^{-1} in D_2O). The VA spectrum[10] also shows one peak around 1634 cm^{-1} in this region for deuterated AAMA in D_2O. Therefore, although the C_7^{eq} conformer is the lowest energy structure among the eight conformers within the SCRF models, there is no explicit water considered and no experimental data to support the conclusion that the intramolecular seven-atom-ring structure is still the most stable conformation for AAMA in aqueous solutions.

3.1.2. AAMA with Explicit Water Molecules. Figure 1a−g shows the final optimized AAMA+4H_2O structures. The ϕ, ψ angles and the relative energies, ΔE, of these conformers are given in the lower part of Table 1. After optimization our initial C_7^{eq}+4H_2O and C_5^{ext}+4H_2O conformers converged to one structure, which we call the P_{II} structure and corresponds to the "β" ($\phi = -80°$, $\psi = 120°$) structure in ref 7. Since the ϕ and ψ angles of the AAMA+4H_2O conformers are not the same as those in isolated state structures, we call our optimized AAMA+4H_2O conformers P_{II}, β_2', $C_7^{ax'}$, α_R', α_L', α_D', and α_P'. For comparison we have also included the AAMA+4H_2O conformer reported by Jalkanen and Suhai,[1] designated "Crystal", because the H_2O molecules were added according to the H-bonding directions in the AAMA crystal.[46] Note that the ϕ and ψ angles for this structure are very similar to those of the P_{II} structure. These two structures show how small changes of the positions of the water molecules around (H-bonding with) AAMA can affect the structural properties, relative energies, and also vibrational properties of AAMA.

The P_{II} conformer is the most stable structure among our AAMA+4H_2O conformers. The relative energy ordering for the other structures is β_2', α_R', and α_L'. Here again we see that water substantially changes the energy differences between peptide conformers. Similar results were reported earlier for the different (methyl) conformers of *N*′-methylacetamide.[48−49]

After we reoptimized the AAMA+4H_2O structures in our model 5, the P_{II} and α_R' conformers turn out to be the most stable structures, and the α_L' conformer was further stabilized and became even more stable than the β_2' conformer.

From the point of view of the dipole moment, Brooks et al.[8,22] stated that, because of the large net molecular dipole moment of the helical structures, the α_R and α_L structures tend to show more favorable solvation energies than do the C_7 structures and, hence, are significantly stabilized in aqueous solutions.

The geometries of four of the AAMA conformers in model 5 are given in Table 2. Compared with the isolated state AAMA structures,[1] we found that H-bonding with the water molecules caused the O_5═C_1 and O_{18}═C_{10} bonds to lengthen and the two peptide bonds, C_1−N_2 and C_{10}−N_{16}, to shorten. On average, the lengthening of the C═O bonds is about 0.014 Å, and the shortening of the peptide C−N bonds is about 0.016 Å. Since now the two C═O and two N−H bonds in the P_{II} structure all have H-bonding with the water molecules, the two bond lengths of each type are nearly the same. The two N−H bonds in this structure are also longer than those in the gas-phase C_7^{eq} structure by about 0.015 Å.

When there are no explicit water molecules, i.e., in the first three models, the α_R conformer cannot be localized. But it can be stabilized and even turns out to be one of the most stable

TABLE 2: B3LYP/6-31G* Optimized Geometries (Å and deg) for Four Conformers of AAMA+4H_2O in the Onsager Solvent Model

geometry[a]	β'_2	α'_L	α'_R	P_{II}
$r(C_1{=}O_5)$	1.2432	1.2388	1.2403	1.2408
$r(C_1{-}N_2)$	1.3489	1.3580	1.3539	1.3498
$r(C_1{-}C_3)$	1.5182	1.5171	1.5166	1.5185
$r(N_2{-}C_4)$	1.4632	1.4697	1.4579	1.4575
$r(C_4{-}C_{10})$	1.5329	1.5524	1.5469	1.5432
$r(C_4{-}C_{12})$	1.5370	1.5287	1.5339	1.5352
$r(C_{10}{=}O_{18})$	1.2423	1.2403	1.2385	1.2434
$r(C_{10}{-}N_{16})$	1.3396	1.3460	1.3506	1.3392
$r(N_{16}{-}C_{17})$	1.4548	1.4547	1.4551	1.4541
$r(N_2{-}H_6)$	1.0296	1.0140	1.0256	1.0290
$r(C_4{-}H_{11})$	1.0906	1.0966	1.0923	1.0923
$r(N_{16}{-}H_{19})$	1.0302	1.0237	1.0172	1.0292
$r(C_3{-}H_8)$	1.0939	1.0926	1.0935	1.0947
$r(C_3{-}H_7)$	1.0920	1.0958	1.0923	1.0953
$r(C_3{-}H_9)$	1.0960	1.0928	1.0955	1.0923
$r(C_{12}{-}H_{13})$	1.0934	1.0905	1.0951	1.0948
$r(C_{12}{-}H_{14})$	1.0963	1.0931	1.0946	1.0950
$r(C_{12}{-}H_{15})$	1.0941	1.0944	1.0950	1.0947
$r(C_{17}{-}H_{20})$	1.0971	1.0904	1.0905	1.0958
$r(C_{17}{-}H_{21})$	1.0919	1.0951	1.0967	1.0950
$r(C_{17}{-}H_{22})$	1.0937	1.0949	1.0944	1.0918
$\theta(O_5{-}C_1{-}N_2)$	123.88	122.47	122.90	124.07
$\theta(C_1{-}N_2{-}C_4)$	121.83	123.00	121.86	123.38
$\theta(N_2{-}C_4{-}C_{10})$	108.57	112.13	113.31	110.74
$\theta(C_4{-}C_{10}{-}O_{18})$	119.88	121.10	120.05	121.95
$\theta(C_4{-}C_{10}{-}N_{16})$	116.31	114.86	116.57	115.73
$\theta(N_2{-}C_1{-}C_3)$	116.06	115.88	115.94	115.55
$\theta(N_2{-}C_4{-}C_{12})$	111.56	112.58	110.11	110.14
$\theta(C_{10}{-}C_4{-}C_{12})$	109.96	111.77	110.71	109.72
$\theta(C_{10}{-}N_{16}{-}C_{17})$	121.27	123.31	122.06	121.14
$\theta(C_1{-}N_2{-}H_6)$	118.88	115.87	118.89	118.15
$\theta(C_4{-}N_2{-}H_6)$	119.17	117.04	119.21	118.29
$\theta(C_{10}{-}C_4{-}H_{11})$	110.00	106.40	104.32	108.77
$\theta(C_{10}{-}N_{16}{-}H_{19})$	120.00	119.30	119.92	120.36
$\theta(C_1{-}C_3{-}H_8)$	108.37	108.80	109.28	108.47
$\theta(C_1{-}C_3{-}H_7)$	112.95	108.26	113.05	108.75
$\theta(C_1{-}C_3{-}H_9)$	108.90	113.22	107.73	113.01
$\theta(H_7{-}C_3{-}H_8)$	109.76	108.40	110.09	107.17
$\theta(H_8{-}C_3{-}H_9)$	107.10	109.71	107.79	109.59
$\theta(H_7{-}C_3{-}H_9)$	109.59	108.35	108.74	109.68
$\theta(C_4{-}C_{12}{-}H_{13})$	110.10	110.48	111.14	110.88
$\theta(C_4{-}C_{12}{-}H_{14})$	110.64	109.87	110.09	110.44
$\theta(C_4{-}C_{12}{-}H_{15})$	109.66	109.51	110.27	110.20
$\theta(H_{13}{-}C_{12}{-}H_{14})$	108.45	108.53	108.42	107.92
$\theta(H_{13}{-}C_{12}{-}H_{15})$	109.28	109.34	108.24	108.80
$\theta(N_{16}{-}C_{17}{-}H_{20})$	111.63	108.76	108.35	111.13
$\theta(N_{16}{-}C_{17}{-}H_{21})$	108.57	109.70	111.15	110.83
$\theta(N_{16}{-}C_{17}{-}H_{22})$	110.22	110.98	109.66	108.34
$\theta(N20{-}C_{17}{-}H_{21})$	108.97	109.09	109.28	107.84
$\theta(H_{20}{-}C_{17}{-}H_{22})$	107.99	109.65	109.45	109.23
$\phi(C_1{-}N_2{-}C_4{-}C_{10})$	−151.95	59.08	−80.27	−92.74
$\psi(N_2{-}C_4{-}C_{10}{-}N_{16})$	118.41	52.45	−47.61	128.61

[a] Atoms numbered as in Figure 1a.

structures when explicit water molecules are added. If we take the AAMA geometry of the P_{II} conformer and reoptimize its geometry in models 2 and 3, we found that it changed back to the C_7^{eq} conformer in the Onsager model and to the C_5^{ext} conformer in the SCIPCM model. Therefore, the explicit water molecules may influence the solute conformations immensely and should be considered when hydration effects are studied.

3.2. Spectral Analysis of the Conformers with Explicit Water Molecules. The conformers we calculated do not sample the whole $\phi-\psi$ map. The orientations of the water molecules also influence the relative energies. We can see in models 4 and 5 that the P_{II} and "Crystal" conformers have similar ϕ and ψ angles but very different water orientations and different relative energies. Therefore, just according to the energy comparisons between the conformers, we cannot say which conformer is the structure of AAMA in water solution. We therefore calculated the VA, Raman, and VCD spectra of the four lowest energy geometries (i.e., β'_2, α'_L, α'_R, and P_{II}) obtained in models 4 and 5. Using the same Hessians but replacing hydrogens with deuteriums, we also obtained the VA, Raman, and VCD spectra for the four deuterated conformers with four D_2O molecules in models 4 and 5. We also calculated the ROA spectra for four AAMA conformers obtained from model 5.

Some groups have scaled the RHF/4-31G quantum mechanical force field (QMFF),[49] the RHF/4-31G* QMFF,[47] and the RHF/6-31+G* QMFF,[48] to the experimentally observed anharmonic frequencies to produce a scaled quantum mechanical force field (SQMFF). We have also scaled RHF/6-31G** and RHF/3-21G QMFFs for 2-oxetanone.[50] The scale factors were then transferred to 4-methyl-2-oxetanone to predict the VA and VCD spectra. The SQMFF was in much better agreement with the experimentally observed VA and VCD spectra than the QMFF or uniformed scaled quantum mechanical force field (USQMFF). Clearly starting from any internal coordinate force field one can scale (or parametrize) it and get better agreement with the experimental frequencies. Our work shows that looking only at the rms difference between frequencies can be very misleading. By comparing the calculated and observed VA and VCD intensites, we were able to show that the intensities are very sensitive to the scaling, while the frequencies are not.[50] Note that the experimentally observed frequencies are anharmonic, but the calculated frequencies are harmonic. Most of the scaling of QMFF to produce SQMFF has been done on the RHF level QMFF, which is substantially lower in accuracy than MP2 and B3LYP level force fields.

With the problems just mentioned we have decided to perform higher level calculations, here at the B3LYP/6-31G* level of theory. The hope here is that at this level the nonuniqueness problem of scaling force fields to experimental data could be alleviated. The Stephens group in Los Angeles, CA, and others have well documented that both the MP2 and B3LYP level force fields are much more accurate than RHF force fields and have also shown that they are of adequate accuracy to predcit accurately the VA and VCD spectra of molecules when combined with accurate APT and DOG AAT.[51−56]

In this paper we will compare the ab initio frequencies and intensities to the experimentally observed anharmonic frequencies and intensities. The goal here is not to get the best agreement with experiment and to transfer scale factors to other molecules as Williams[49] and Krimm[47,48] have done, but to see how well one can do in accurately predicting the VA, VCD, Raman, and ROA spectra at the B3LYP/6-31G* level of theory.

The Cartesian force constants have been transformed into internal coordinates, which allows us to use potential energy distributions to help in the assignment of the normal modes. In Table 3 we give our internal coordinates for the P_{II}+4H_2O complex. The first 60 internal coordinates are what one would use if one performs the vibrational analysis only for AAMA. With the addition of the four water molecules we now have 36 more internal coordinates. Each water molecule has three internal coordinates, corresponding to the three vibrational frequencies of the water molecule. Hence 12 of these 36 coordinates correspond to the internal coordinates of the four water molecules. That leaves 24 internal coordinates which relate to the H-bond coupling movements between the water molecules and the AAMA. To our knowledge no one has yet determined a good set of internal coordinates to represent what we call "coupling modes" between the AAMA and the four water molecules. This also creates a problem when one would

TABLE 3: Internal Coordinate Definitions for P_{II} with Four Water Molecules

coord	definition	description[a]	coord	definition	description[a]
Q_1	$\Delta r_{1,2}$	C_1-N_2 s	Q_{48}	$(1/\sqrt{18})\,(4\Delta\theta_{2,4,12}+\Delta\theta_{2,4,10}+\Delta\theta_{10,4,12})$	$C_2C_4C_{12}$ d
Q_2	$\Delta r_{1,3}$	C_1-C_3 s	Q_{49}	$(1/\sqrt{18})\,(4\Delta\theta_{10,4,12}+\Delta\theta_{2,4,10}+\Delta\theta_{2,4,12})$	$C_{10}C_4C_{12}$ d
Q_3	$\Delta r_{1,5}$	$C_1=O_5$ s	Q_{50}	$(1/\sqrt{6})\,(2\Delta\theta_{3,1,2}-\Delta\theta_{3,1,5}-\Delta\theta_{2,1,5})$	$C_3C_1N_2$ d
Q_4	$\Delta r_{2,4}$	N_2-C_4 s	Q_{51}	$(1/\sqrt{6})\,(2\Delta\theta_{4,10,16}-\Delta\theta_{18,10,4}-\Delta\theta_{18,10,16})$	$C_4C_{10}N_{16}$ d
Q_5	$\Delta r_{2,5}$	N_2-H_5 s	Q_{52}	$(1/\sqrt{6})\,(2\Delta\theta_{1,2,4}-\Delta\theta_{6,2,4}-\Delta\theta_{6,2,1})$	$C_1N_2C_4$ d
Q_6	$\Delta r_{3,7}$	C_3-H_7 s	Q_{53}	$(1/\sqrt{6})\,(2\Delta\theta_{10,16,17}-\Delta\theta_{19,16,10}-\Delta\theta_{19,16,17})$	$C_{10}N_{16}C_{17}$ d
Q_7	$\Delta r_{3,8}$	C_3-H_8 s	Q_{54}	$\tau_{3,1}$	C_3-C_1 t
Q_8	$\Delta r_{3,9}$	C_3-H_9 s	Q_{55}	$\tau_{1,2}$	C_1-N_2 t
Q_9	$\Delta r_{4,10}$	C_4-C_{10} s	Q_{56}	$\tau_{2,4}$	N_2-C_4 t
Q_{10}	$\Delta r_{4,11}$	C_4-H_{11} s	Q_{57}	$\tau_{4,12}$	C_4-C_{12} t
Q_{11}	$\Delta r_{4,12}$	C_4-C_{12} s	Q_{58}	$\tau_{4,10}$	C_4-C_{10} t
Q_{12}	$\Delta r_{10,16}$	$C_{10}-N_{16}$ s	Q_{59}	$\tau_{10,16}$	$C_{10}-N_{16}$ t
Q_{13}	$\Delta r_{10,18}$	$C_{10}=O_{18}$ s	Q_{60}	$\tau_{16,17}$	$N_{16}-C_{17}$ t
Q_{14}	$\Delta r_{12,13}$	$C_{12}-H_{13}$ s	Q_{61}	$\Delta r_{23,24}$	$H_{23}-O_{24}$ s
Q_{15}	$\Delta r_{12,14}$	$C_{12}-H_{14}$ s	Q_{62}	$\Delta r_{25,24}$	$H_{25}-O_{24}$ s
Q_{16}	$\Delta r_{12,15}$	$C_{12}-H_{15}$ s	Q_{63}	$\Delta\theta_{23,24,25}$	$H_{23}O_{24}H_{25}$ b
Q_{17}	$\Delta r_{16,17}$	$N_{16}-C_{17}$ s	Q_{64}	$\Delta r_{5,23}$	$O_5\cdots H_{23}$ s
Q_{18}	$\Delta r_{16,19}$	$N_{16}-H_{19}$ s	Q_{65}	$\Delta\theta_{1,5,23}$	$C_1O_5H_{23}$ b
Q_{19}	$\Delta r_{17,20}$	$C_{17}-H_{20}$ s	Q_{66}	$\tau_{1,5}$	$C_1=O_5$ t
Q_{20}	$\Delta r_{17,21}$	$C_{17}-H_{21}$ s	Q_{67}	$\Delta\theta_{5,23,24}$	$O_5H_{23}O_{24}$ b
Q_{21}	$\Delta r_{17,22}$	$C_{17}-H_{22}$ s	Q_{68}	$\tau_{5,23}$	$O_5\cdots H_{23}$ t
Q_{22}	$(1/\sqrt{2})\,(\Delta\theta_{6,2,1}-\Delta\theta_{6,2,4})$	H_6-N_2 ip	Q_{69}	$\tau_{23,24}$	$H_{23}-O_{24}$ t
Q_{23}	$(1/\sqrt{2})\,(\Delta\theta_{19,16,17}-\Delta\theta_{19,16,10})$	$H_{19}-N_{16}$ ip	Q_{70}	$\Delta r_{26,6}$	$O_{26}\cdots H_6$ s
Q_{24}	$\delta_{6,2}$	H_6-N_2 op	Q_{71}	$\Delta\theta_{26,6,2}$	$O_{26}H_6N_2$ b
Q_{25}	$\delta_{19,16}$	$H_{19}-N_{16}$ op	Q_{72}	$\tau_{6,2}$	H_6-N_2 t
Q_{26}	$(1/\sqrt{2})\,(\Delta\theta_{3,1,5}-\Delta\theta_{2,1,5})$	$O_5=C_1$ ip	Q_{73}	$\Delta r_{27,26}$	$H_{27}-O_{26}$ s
Q_{27}	$(1/\sqrt{2})\,(\Delta\theta_{18,10,16}-\Delta\theta_{18,10,4})$	$O_{18}=C_{10}$ ip	Q_{74}	$\Delta\theta_{27,26,6}$	$H_{27}O_{26}H_6$ b
Q_{28}	$\delta_{5,1}$	$O_5=C_1$ op	Q_{75}	$\tau_{26,6}$	$O_{26}\cdots H_6$ t
Q_{29}	$\delta_{18,10}$	$O_{18}=C_{10}$ op	Q_{76}	$\Delta r_{28,26}$	$H_{28}-O_{26}$ s
Q_{30}	$(1/\sqrt{6})\,(\Delta\theta_{7,3,8}+\Delta\theta_{7,3,9}+\Delta\theta_{8,3,9})$ $-\Delta\theta_{7,3,1}-\Delta\theta_{8,3,1}-\Delta\theta_{9,3,1})$	$C_1C_3H_{7,8,9}$ sb	Q_{77}	$\Delta\theta_{28,26,27}$	$H_{28}O_{26}H_{27}$ b
			Q_{78}	$\Delta\theta_{28,26,6}$	$H_{28}\ O_{26}\ H_6$ b
Q_{31}	$(1/\sqrt{6})\,(2\Delta\theta_{7,3,8}-\Delta\theta_{7,3,9}-\Delta\theta_{8,3,9})$	$C_3H_{7,8,9}$ ab	Q_{79}	$\Delta r_{29,18}$	$H_{29}\cdots O_{18}$ s
Q_{32}	$(1/\sqrt{2})\,(\Delta\theta_{7,3,9}-\Delta\theta_{8,3,9})$	$C_3H_{7,8,9}$ ab′	Q_{80}	$\Delta\theta_{29,18,10}$	$H_{29}O_{18}C_{10}$ b
Q_{33}	$(1/\sqrt{6})\,(2\Delta\theta_{9,3,1}+\Delta\theta_{8,3,1}+\Delta\theta_{7,3,1})$	$C_1C_3H_{7,8,9}$ r	Q_{81}	$\tau_{18,10}$	$O_{18}=C_{10}$ t
Q_{34}	$(1/\sqrt{2})\,(\Delta\theta_{8,3,1}-\Delta\theta_{7,3,1})$	$C_1C_3H_{7,8,9}$ r′	Q_{82}	$\Delta r_{29,30}$	$H_{29}-O_{30}$ s
Q_{35}	$(1/\sqrt{6})\,(\Delta\theta_{13,12,14}+\Delta\theta_{13,12,15}+\Delta\theta_{14,12,15})$ $-\Delta\theta_{15,12,4}-\Delta\theta_{14,12,4}-\Delta\theta_{13,12,4})$	$C_4C_{12}H_{13,14,15}$ sb	Q_{83}	$\Delta\theta_{30,29,18}$	$O_{30}H_{29}O_{18}$ b
			Q_{84}	$\tau_{29,18}$	$H_{29}\cdots O_{18}$ t
Q_{36}	$(1/\sqrt{6})\,(\Delta\theta_{13,12,14}+\Delta\theta_{13,12,15}+\Delta\theta_{14,12,15})$	$C_{12}H_{13,14,15}$ ab	Q_{85}	$\Delta r_{31,30}$	$H_{31}-O_{30}$ s
Q_{37}	$(1/\sqrt{2})\,(\Delta\theta_{13,12,15}-\Delta\theta_{14,12,15})$	$C_{12}H_{13,14,15}$ ab′	Q_{86}	$\Delta\theta_{31,30,29}$	$H_{31}O_{30}H_{29}$ b
Q_{38}	$(1/\sqrt{6})\,(2\Delta\theta_{15,12,4}-\Delta\theta_{14,12,4}-\Delta\theta_{13,12,4})$	$C_4C_{12}H_{13,14,15}$ r	Q_{87}	$\tau_{30,29}$	$O_{30}-H_{29}$ t
Q_{39}	$(1/\sqrt{2})\,(\Delta\theta_{14,12,4}-\Delta\theta_{13,12,4})$	$C_4C_{12}H_{13,14,15}$ r′	Q_{88}	$\Delta r_{19,32}$	$H_{19}\cdots O_{32}$ s
Q_{40}	$(1/\sqrt{6})\,(\Delta\theta_{20,17,21}+\Delta\theta_{20,17,22}+\Delta\theta_{21,17,22})$ $-\Delta\theta_{22,17,16}-\Delta\theta_{21,17,16}-\Delta\theta_{20,17,16})$	$N_{16}C_{17}\ H_{20,21,22}$ sb	Q_{89}	$\Delta\theta_{32,19,16}$	$O_{32}H_{19}N_{16}$ b
			Q_{90}	$\tau_{19,16}$	$H_{19}-N_{16}$ t
Q_{41}	$(1/\sqrt{6})\,(2\Delta\theta_{20,17,22}-\Delta\theta_{21,17,22})$	$C_{17}H_{20,21,22}$ ab	Q_{91}	$\Delta r_{33,32}$	$H_{33}-O_{32}$ s
Q_{42}	$(1/\sqrt{2})\,(\Delta\theta_{20,17,21}+\Delta\theta_{20,17,22}+\Delta\theta_{21,17,22})$	$C_{17}\ H_{20,21,22}$ ab′	Q_{92}	$\Delta\theta_{33,32,19}$	$H_{33}O_{32}H_{19}$ b
Q_{43}	$(1/\sqrt{6})\,(\Delta\theta_{22,17,16}-\Delta\theta_{21,17,16}-\Delta\theta_{20,17,16})$	$N_{16}C_{17}H_{20,21,22}$ r	Q_{93}	$\tau_{32,19}$	$O_{32}\cdots H_{19}$ t
Q_{44}	$(1/\sqrt{2})\,(\Delta\theta_{21,17,16}-\Delta\theta_{20,17,16})$	$N_{16}C_{17}H_{20,21,22}$ r′	Q_{94}	$\Delta r_{34,32}$	$H_{34}-O_{32}$ s
Q_{45}	$(1/\sqrt{6})\,(2\Delta\theta_{11,4,2}-\Delta\theta_{11,4,10}-\Delta\theta_{11,4,12})$	C_4-H_{11} r	Q_{95}	$\Delta\theta_{34,32,33}$	$H_{34}O_{32}H_{33}$ b
Q_{46}	$(1/\sqrt{2})\,(\Delta\theta_{11,4,10}-\Delta\theta_{11,4,12})$	C_4-H_{11} r′	Q_{96}	$\Delta\theta_{34,32,19}$	$H_{34}O_{32}H_{19}$ b
Q_{47}	$(1/\sqrt{18})\,(4\Delta\theta_{2,4,10}+\Delta\theta_{2,4,12}+\Delta\theta_{10,4,12})$	$C_2C_4C_{10}$ d			

[a]Atoms numbered as in Figure 1a. s = stretch. d = deformation. b = bend. ip = in-plane. op = out-of-plane. sb = symmetric bend. ab = antisymmetric bend. t = torsion. r = rock.

like to scale the ab initio QMFF. What set of internal coordinates does one use for the scaling of these modes? Again the question of which data to include in the scaling, the anharmonicity of frequencies, and effects of solvent are all problems that add to the nonuniqueness of the parametrization process.

The question of the scaling of QMFF calculated for complexes with many water molecules is still an open ended question that is beyond the scope of this work. People who have attempted to address this problem have run into problems, and most have just neglected the force constants for the waters and the coupling modes and have scaled only the force constants for the solute.

3.2.1. Influence of H_2O Molecules on the Vibrational Spectra of AAMA. To show the effect of neglecting the water and coupling mode force constants on the vibrational frequencies and on the VA, Raman, and VCD intensities, in Table 4 we present the vibrational frequencies and VA, Raman, and VCD intensities of the P_{II}+4H_2O+Onsager complex using the full Hessian and full tensors (see note *c*) and then using the approximation of throwing away the water and coupling mode force constants from the Hessian and tensors (see note *d*). We also present the corresponding spectra in Figure 2. The spectra with superscript *a* are for the real P_{II}+4H_2O+Onsager conformer, and those with superscript *b* are obtained by deleting the water and the coupling components from the Hessian, APT,

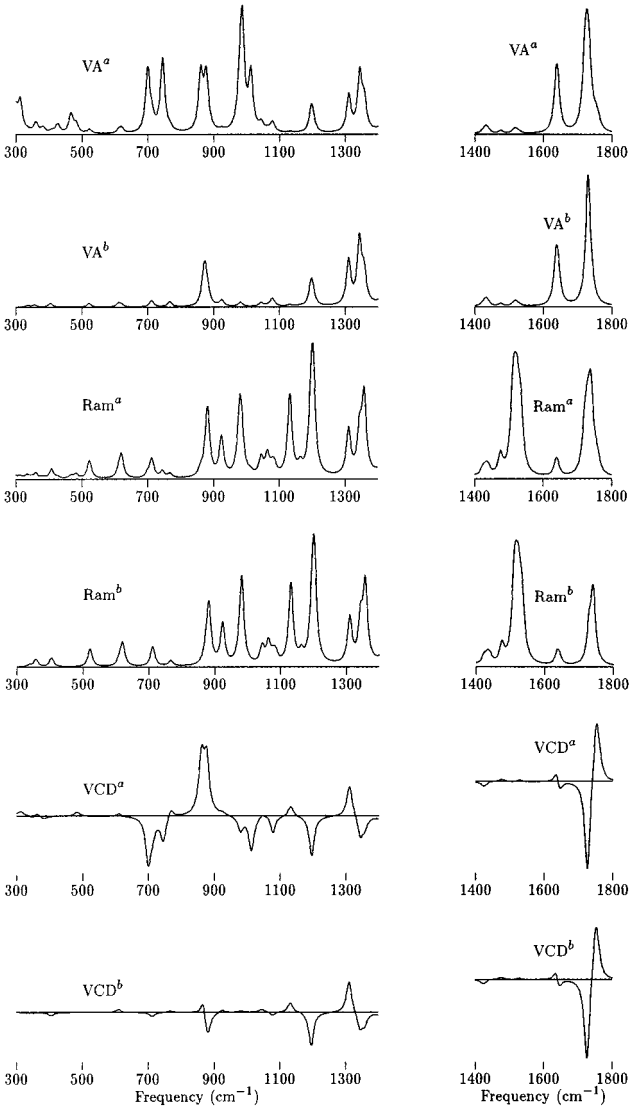

Figure 2. (a) IR, Raman and VCD spectra for P_{II}+4H_2O+Onsager conformer (see note *c* of Table 4). (b) Only the geometry of AAMA was taken from the P_{II}+4H_2O+Onsager conformer. IR, Raman, and VCD spectra are calculated through deleting the water and the coupling components from Hessian, APT, AAT, and EDEDPD (see note d of Table 4).

AAT, and EDEDPD. As one can see in Table 4, we obtain more normal modes in amide I and in the low-frequency region for AAMA+4H_2O than for the isolated AAMA molecule. In the amide I region (C═O stretching), there are six normal frequencies from 1800 to 1700 cm^{-1} for P_{II}+4H_2O. Further potential energy distribution analysis shows that these modes are mainly connected to the water bending, H-bond rotating, and C═O stretching. The studies of Sieler et al. show that the vibrational coupling between the amide I modes of some peptides and the bending modes of the surrounding water molecules provides a continuumm of vibrational states.[16] When we delete the water and the coupling components from the Hessian, APT, and AAT, we only obtain two amide I modes with frequencies 1742 and 1731 cm^{-1}. The VA intensity for the mode 1731 cm^{-1} and the VCD intensity for 1742 cm^{-1} are extremly intense and very different from any of the original six modes. Now one cannot say which two of the six modes belong to the amide I modes. The C═O stretching and the water bending are vibrationally coupled.

From Table 4 and Figure 2, one can see that the Raman spectrum after deleting the water and the coupling components

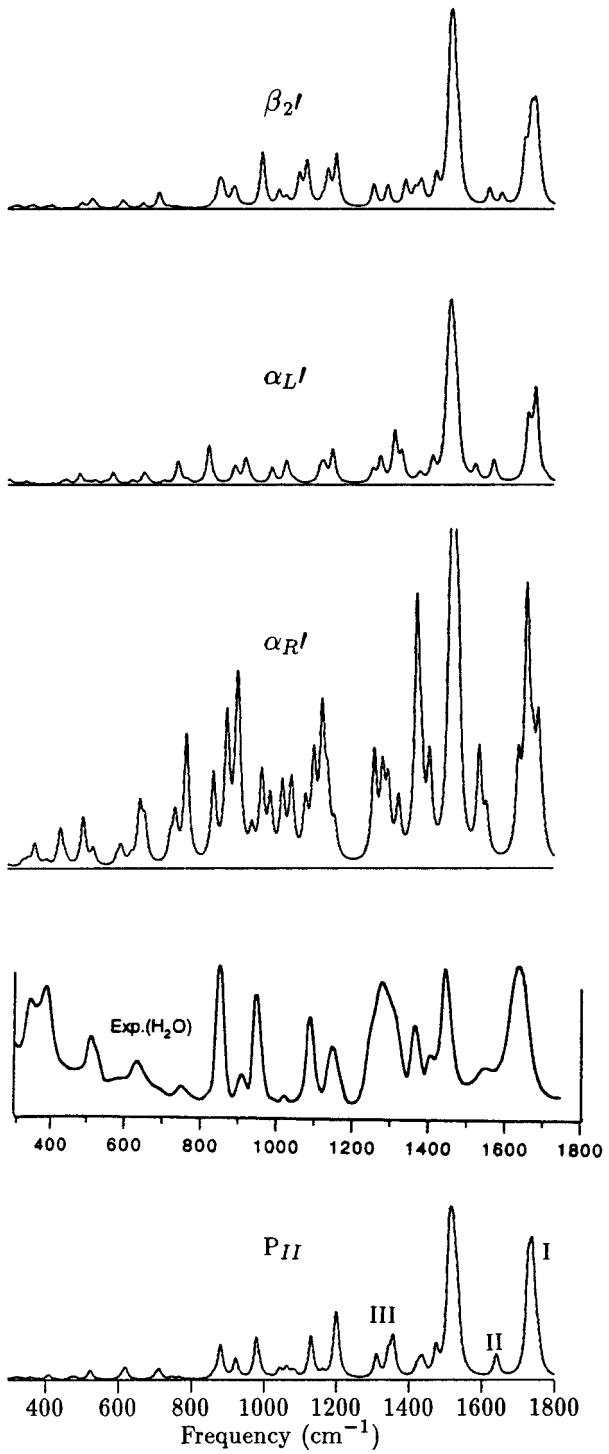

Figure 3. Experimental vibrational Raman spectrum of AAMA in H_2O solution (from ref 13) and calculated Raman spectra of β_2'+4H_2O, α_L'+4H_2O, α_R'+4H_2O, and P_{II}+4H_2O.

from the Hessian and EDEDPD does not have significant changes in the whole region of 1800−300 cm^{-1}. But the VA[b] and VCD[b] spectra are very different from the VA[a] and VCD[a] spectra in the lower frequency region below 1100 cm^{-1}. The water molecules change the dipole moment of the AAMA and therefore influence the VA and VCD spectra of the AAMA significantly. The AAMA EDEDPs, however, are not strongly influenced by the H_2O molecules; therefore the shape of Raman spectrum Ram[b] is very similar to that of Ram[a].

In the next section we will present our Raman and VCD calculations using the full Hessians and the complete tensors.

TABLE 4: Vibrational Properties for P_{II} Conformer Obtained in the Onsager Solvent Model[a]

amide modes	obs Ram[b]	P_{II} with 4 H_2O[c] freq	VA	Ram	VCD	assignment	P_{II} without 4 H_2O[d] freq	VA	Ram	VCD	assignment
		1760	64.7	2.7	15.0	$Q_{84,87}$					
I		1751	64.1	2.7	72.4	$Q_{68,69,95}Q_3$					
I	1650	1739	68.7	17.1	1.2	$Q_{84,87}Q_{3,22,13}$	1742	69.2	18.1	112.7	$Q_{3,13,22,1}$
I		1733	280.5	7.4	26.4	$Q_{68,69,63}Q_{3,22,13}$					
I		1728	396.6	7.4	−132.7	$Q_{84,87}Q_{13}$	1731	886.4	8.6	−143.2	$Q_{13,3,12}$
		1721	415.7	9.9	−5.6	$Q_{84,87}$					
II		1643	219.2	2.1	−28.6	$Q_{93,90}$ Q_{23}	1643	200.0	1.9	−21.3	$Q_{23,12}$
II	1552	1638	328.4	3.3	29.5	$Q_{22,1}$ $Q_{72,75,71}$	1637	304.3	2.9	25.7	$Q_{22,1}$
		1536	1.1	11.2	−1.7	Q_{41}	1536	1.0	11.3	−1.5	$Q_{41,43}$
		1530	9.9	8.1	3.2	$Q_{36,37}$	1530	9.0	8.0	2.6	$Q_{36,37,38}$
		1524	6.2	13.5	0.2	$Q_{37,36}$	1524	6.2	13.4	1.1	$Q_{37,36,39}$
		1519	24.8	6.2	0.3	$Q_{31,32}$	1519	26.1	6.5	0.4	$Q_{31,32,33}$
		1515	12.1	9.0	0.3	$Q_{32,31}$	1515	11.7	9.0	−0.6	$Q_{32,31,34}$
	1458	1511	9.4	16.2	−1.4	$Q_{42,44}$	1511	9.3	16.2	−1.5	$Q_{42,44}$
	1420	1476	26.2	6.0	3.2	$Q_{40}Q_{93,90}$	1476	23.5	5.6	3.3	Q_{40}
		1441	13.7	2.1	1.3	$Q_{35}Q_{93,90}$	1441	14.4	2.1	0.9	$Q_{35,45}$
	1381	1433	58.3	2.4	−1.1	$Q_{30,2}$	1433	61.2	2.4	−1.2	$Q_{30,2}$
		1424	20.8	2.2	−6.5	$Q_{93,90}Q_{46,35}$	1424	22.1	2.3	−6.9	$Q_{35,46,45}$
III	1324	1358	45.5	9.5	−4.1	$Q_{45,26,1}$	1358	47.5	9.5	−5.4	$Q_{45,1,46}$
III	1296	1344	91.6	5.0	−8.4	$Q_{75,72}Q_{22,45,1}$	1344	101.9	5.0	−7.4	$Q_{45,1,22}$
III	1272	1311	60.6	5.7	13.4	$Q_{93,90}Q_{46,23,12}$	1311	73.1	5.7	15.5	$Q_{46,12,23}$
	1164	1203	13.2	12.5	3.2	$Q_{93,90}Q_{43,53}$	1203	14.0	12.4	4.7	Q_{43}
		1197	43.5	8.3	−20.8	$Q_{4,52}Q_{75,72}$	1197	41.2	7.8	−21.4	$Q_{4,39,48}$
		1164	0.8	1.3	0.1	$Q_{93,90}Q_{44}$	1163	1.1	1.4	0.7	$Q_{44,42}$
	1107	1132	2.6	11.9	5.2	$Q_{11,52,49,38}$	1132	3.3	11.8	5.5	$Q_{11,38,4}$
		1086	1.3	1.3	1.7	$Q_{38,34,4}$	1086	1.7	1.7	0.5	$Q_{38,34,33}$
		1079	19.0	1.2	−10.1	$Q_{72,75}Q_{34,28}$	1079	15.4	1.2	−2.4	$Q_{34,28}$
	1036	1064	4.5	3.2	1.4	$Q_{17,27}$ $Q_{75,72}$	1064	1.9	3.3	0.4	Q_{17}
	1003	1045	16.3	2.8	2.10	$Q_{72,75}$ Q_{33}	1045	8.0	2.7	1.8	$Q_{33,11}$
		1013	120.8	0.5	−18.8	$Q_{75,72}$					
		987	220.1	4.4	0.4	$Q_{93,90}$					
	960	980	84.4	11.2	−8.4	$Q_{93,90,75}Q_2$	982	9.7	15.1	0.8	$Q_{2,11}$
	922	925	4.8	7.0	1.2	$Q_{75,72}Q_{52}$	925	14.3	7.3	1.9	$Q_{39,52,4}$
	864	882	18.0	11.9	−4.2	$Q_{75,72}Q_{51}$	883	21.2	11.0	−12.3	$Q_{9,51,43}$
		877	124.4	1.8	36.2	$Q_{93,90}$	875	75.3	1.7	−14.6	$Q_{59,25}$
		861	143.7	1.2	36.2	$Q_{75,72}$	869	39.8	0.5	19.0	$Q_{55,56,24}$
	760	768	9.0	1.0	6.8	$Q_{93,90}Q_{29}$	767	14.9	1.2	1.2	$Q_{29,47,25}$
		745	212.2	1.5	−18.1	$Q_{84,87}$					
IV	702	713	32.1	4.5	−8.9	$Q_{27,47}Q_{75,72}$	712	20.0	4.6	−3.6	$Q_{27,47,49}$
		700	193.8	1.0	−35.9	$Q_{69,68}$					
IV	644	621	18.1	6.1	−1.0	$Q_{26}Q_{72,75}$	621	8.3	6.0	−0.9	$Q_{26,2}$
		612	12.5	1.6	3.1	$Q_{75,72}Q_{28}$	611	13.1	1.6	3.6	$Q_{28,34}$
	538	524	17.3	5.8	−0.4	$Q_{93,90}Q_{51,50}$	522	16.4	5.7	0.6	$Q_{50,48,51}$
	520	483	39.1	1.6	4.7	$Q_{93,90,68}$					
		468	90.0	1.1	0.1	$Q_{84,87}$					
		427	46.1	0.6	0.1	$Q_{84,87}$					
	395	409	14.1	3.9	−0.3	$Q_{93,69,68}Q_{26,52}$	405	21.7	3.6	−5.3	$Q_{26,50,29}$
	372	383	32.5	0.7	−4.5	$Q_{68,69}$					
		361	58.8	2.5	5.0	$Q_{84,87}$					
	348	348	6.0	0.6	−3.8	$Q_{84,87}$	358	13.7	3.5	−0.6	$Q_{48,53,50}$
		335	10.9	2.0	0.7	$Q_{72,75,90,93}$	336	12.0	0.9	−1.4	$Q_{27,47,53}$
		313	205.1	1.4	7.3	$Q_{72,75,93,90}$					
		304	9.7	0.3	0.4	$Q_{87,84}$					

[a] Frequencies are in cm^{-1}. VA intensities are in km/mol. Raman scattering activities are in $Å^4$ /amu, and VCD intensities are in km/mol. [b] Observed vibrational Raman frequencies for AAMA in H_2O solution are from ref 12. [c] Geometries, frequencies, and atomic polar tensors of $P_{II}+4H_2O$ were obtained using B3LYP/6-31G* method in the Onsager solvent model. Raman scattering activities were calculated with the RHF/6-311+G**/Onsager electric dipole−electric dipole polarizability derivatives. VCD intensities were obtained with the RHF/6-31G* DOG atomic axial tensors. [d] Only the AAMA geometry was taken from the $P_{II}+4H_2O+$Onsager complex. Hessian matrix, atomic polar tensors, atomic axial tensors, and polarizability derivatives were also taken from the corresponding results described in note *c* through deleting the portions relating to the H_2O coordinates.

3.2.2. Raman Spectral Analysis. Now we compare our calculated Raman spectra with the experimental results. We showed the theoretical Raman spectra for the conformers β'_2+4H_2O, α'_L+4H_2O, α'_R+4H_2O, and $P_{II}+4H_2O$ in Figure 3. We see the Raman spectrum of the P_{II} structure is the best comparing with the experimental bands.[13] The spectra of the β'_2 and α'_L conformers are not as good as the spectra of the P_{II} structure for matching the observed bands. The spectrum of the α'_R structure has more split peaks and looks very different from the other three spectra. We then optimized the four AAMA+$4H_2O$ complex structures in model 5. The frequencies and Raman scattering intensities for the $P_{II}+4H_2O+$Onsager complex are given in Table 4. The simulations of these spectra are shown in Figure 4.

On going from model 4 to model 5, the vibrational frequencies of the P_{II} and the β'_2 structures normally do not change by more than 3 cm^{-1}. The largest frequency shifts are only 7 cm^{-1} for the P_{II} conformer and 8 cm^{-1} for the β'_2 conformer,

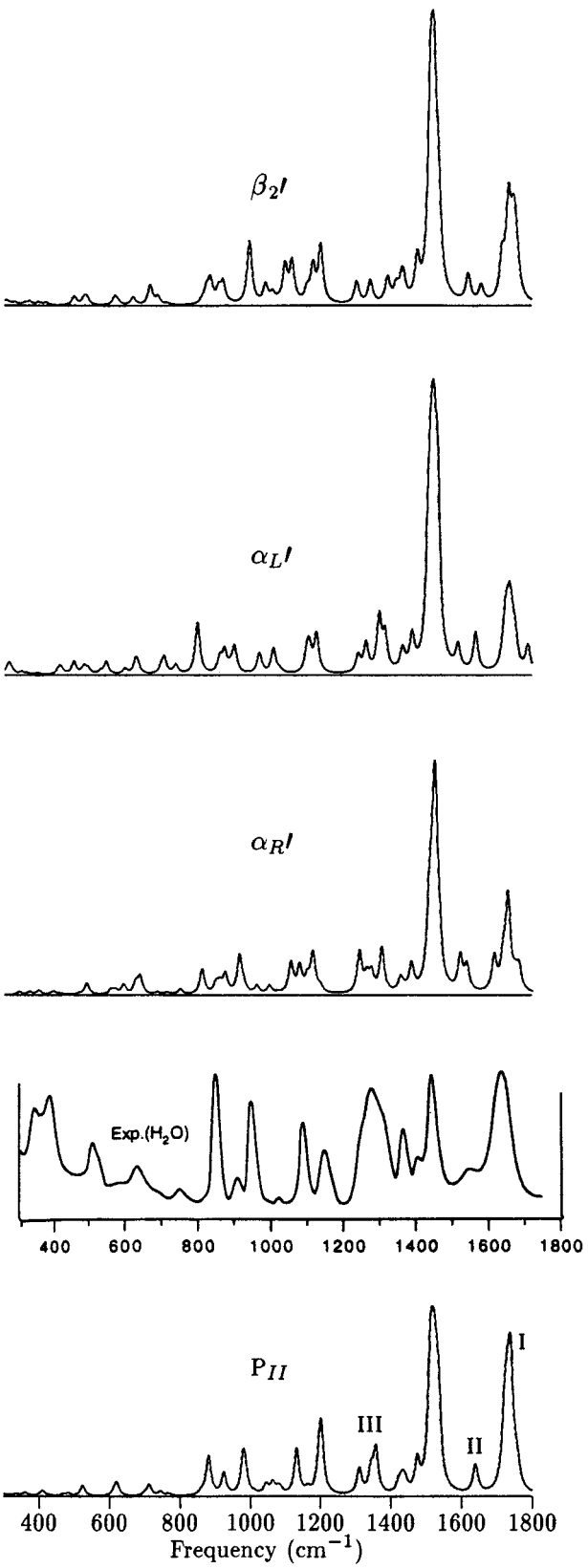

Figure 4. Experimental vibrational Raman spectrum of AAMA in H_2O (from ref 13) and calculated Raman spectra of β_2'+4H_2O, α_L'+4H_2O, α_R'+4H_2O and P_{II}+4H_2O, which are optimized in the Onsager solvent model.

respectively. The frequencies for the α_R' and the α_L' conformers show relatively large changes, up to 28 cm^{-1}. After solvation the intensities of the Raman spectra for the P_{II}, α_L', and β_2' conformers are all strengthened, but for the α_R' they are weakened. The spectrum of the α_R' conformer in Figure 4 shows a big change in comparison with the corresponding spectrum in Figure 3. Here we see that the explicit water molecules can stabilize the α_R' structure of AAMA. Then the solvation model can further modify the orientations of the water molecules, the force field of the complex, and the intensities of vibrational modes.

In Figure 4 we see that the Raman spectrum of the P_{II} structure after solvation still provides the best explanation for the experimental bands. As discussed in the last section, the amide I band (centered at 1739 cm^{-1}) of the P_{II} conformer consists of six normal modes and corresponds to the experimental peak at 1654 cm^{-1} in ref 13 or 1650 cm^{-1} in ref 12. The same region for the other three spectra also consists of six vibrational modes but has split peaks.

The predicted small band around 1640 cm^{-1} in the Raman spectrum for the P_{II} conformer is assigned as an amide II band (N−H deformation and C−N stretching). This matches the experimental band at 1552 cm^{-1} in ref 12. There are two modes in this region for each of the four conformers. The splitting of the two modes is only 5 cm^{-1} for the P_{II} conformer and more than 15 cm^{-1} for the other conformers.

We predict six frequencies for the P_{II} conformer between 1536 and 1511 cm^{-1}, which all represent antisymmetric deformations of the C−CH_3 groups and correspond to the experimental band at 1458 cm^{-1} in ref 12 or 1455 cm^{-1} in ref 13. There are also six normal modes in this region, which form a strong band for the other three conformers.

The predicted modes of 1476 cm^{-1} for P_{II}, 1459 cm^{-1} for α_R', 1460 cm^{-1} for α_L' and 1475 cm^{-1} for β_2' are the symmetric deformation of the N_{16}−CH_3 group. They may correspond to the small observed peak at 1420 cm^{-1} in ref 12. The symmetric C−CH_3 deformation modes at 1441, 1433, and 1424 cm^{-1} for the P_{II} conformer are all relatively weak. But they form a band and correspond to the experimental band at 1381 cm^{-1} in ref 12.

The broad observed band at 1298 cm^{-1} in ref 13 (or 1296 cm^{-1} in ref 12) can be explained by our predicted amide III modes of 1358, 1344, and 1312 cm^{-1} (N−H in-plane bending, C−N stretching, and C_4−H_{11} rocking) for the P_{II} conformer. These three modes split into two bands here.

In the region 1200−800 cm^{-1}, our calculated modes for the P_{II} conformer centered at 1203, 1132, 980, 925, and 882 cm^{-1} can explain the experimental Raman bands at 1164, 1107, 960, 922, and 864 cm^{-1} in ref 12. These modes are mainly produced by the C−C stretching, C−N stretching, C−C−C deformation, C−C−N deformation, C−CH_3 rocking, and N−CH_3 rocking. The spectra of the α_R' and α_L' conformers in this region also show a pattern similar to the experimental curves but not as good as that of the P_{II} conformer. The spectrum of the β_2' conformer is the worst in comparison with the spectra of the other three conformers.

In Figure 5 we present the calculated Raman spectra for these four deuterated AAMA+4D_2O+Onsager conformers. The corresponding data for P_{II}(d) can be found in Table 5. Upon deuteration the D_2O bending modes downshift relative to the H_2O bending modes to around 1260 cm^{-1}. Therefore, we obtained two modes for each conformer in the amide I′ region. The splitting of these two modes for the P_{II} conformer is only 8 cm^{-1}. We therefore obtained one peak around 1730 cm^{-1} for the P_{II} conformer and split peaks for the other three conformers. The amide II modes of the deuterated conformers mix with the antisymmetric deformations of the C−CH_3 groups and form a broad band around 1526 cm^{-1}. The small band at

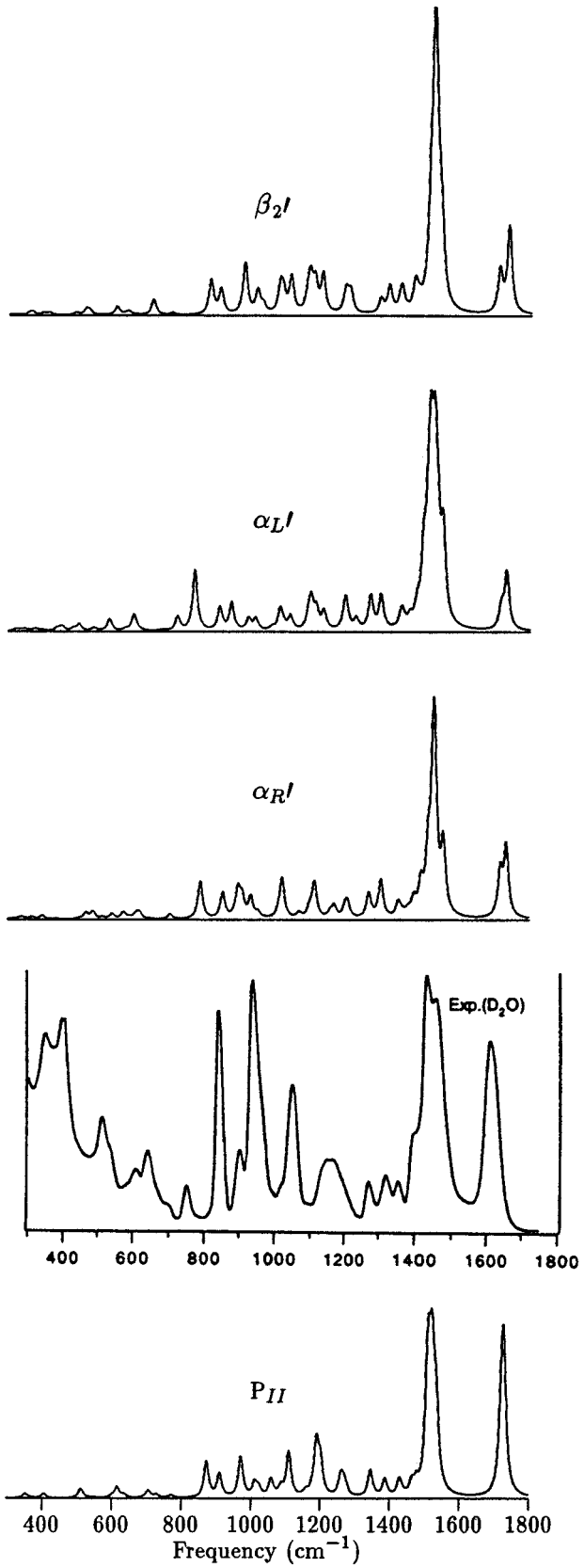

Figure 5. Experimental vibrational Raman spectrum of AAMA in D_2O (from ref 13) and calculated Raman spectra of deuterated β_2'+4D_2O, α_L'+4D_2O, α_R'+4D_2O, and P_{II}+4D_2O, which are optimized in the Onsager solvent model.

1430 cm^{-1} for the P_{II} conformer corresponds to the observed band at 1370 cm^{-1} in ref 12 and relates to the symmetric C−CH_3 deformations. The following two modes at 1388 and 1347 cm^{-1} for the P_{II} structure are assigned to the C_4−H_{11} rocking and H−N in-plane bending modes and correspond to the experimental bands at 1333 and 1287 cm^{-1}, respectively.[12] Roberts et al. measured the VCD spectra in this region and assigned them as the amide III′ bands. We can also find the corresponding bands in the other predicted spectra of β_2', α_L', and α_R' conformers. In the region from 1300 to 800 cm^{-1} we predicted more bands than are experimentally observed.

Both in H_2O and in D_2O solutions we obtained very weak vibrational modes in the lower frequency region. From Table 4 we see that in the lower frequency region there are more vibrational modes of the AAMA+4H_2O structure than for the isolated AAMA structure. These modes are coupled with the movements/vibrations of the H-bonded water molecules. We have only four H_2O (D_2O) molecules in our model, but in aqueous solution there are a large number of water molecules and H-bonds. All the contributions of the H-bonded water movements therefore make the observed Raman spectrum in this region very intense.

To obtain further insights into the conformer distribution problem, we now look at the predicted VCD spectra of the above four conformers and the experimenal VCD spectra of AAMA in H_2O and in D_2O solutions.

TABLE 5: Frequencies (cm^{-1}), Raman Scattering Activities (Å^4/amu), and VCD Intensities (km/mol) of the Deuterated P_{II} Conformer with Four D_2O Molecules in the Onsager Solvent Model

	P_{ii} (d)		
freq	Ram	VCD	assignment
1730	27.1	147.1	$Q_{13,51,12}$
1722	10.0	−159.9	$Q_{3,13,12}$
1539	7.0	−1.0	$Q_{41}Q_{93,90}$
1534	9.5	3.6	$Q_{36,41}$
1526	13.9	7.8	$Q_{31,1,22}$
1524	10.0	−0.4	$Q_{37,36}$
1516	9.3	0.4	$Q_{32,34}$
1514	9.5	−7.3	$Q_{93,90}Q_{23,42}$
1510	12.2	−3.3	$Q_{42}Q_{93,90}$
1479	2.4	1.8	$Q_{22,1,31}$
1466	2.5	−9.7	$Q_{40}Q_{93,90}$
1434	0.9	−6.9	Q_{35}
1430	3.0	0.7	Q_{30}
1388	4.0	−8.1	$Q_{45,46,23}Q_{93,90}$
1347	6.4	13.0	$Q_{46,45,58}$
1276	1.5	−4.0	$Q_{84,87}$
1273	1.1	8.4	$Q_{68,69,95}$
1266	3.3	−10.3	$Q_{68,69,95,63}$
1260	3.4	4.0	$Q_{84,87,77}$
1203	8.5	−10.2	$Q_{93,90}Q_{43}$
1192	13.9	−6.6	$Q_{48,39,52}$
1177	1.0	−4.5	$Q_{22,4}Q_{75,72}$
1160	1.3	1.3	Q_{44}
1112	13.0	8.5	$Q_{93,90}Q_{38}$
1089	2.6	−1.3	$Q_{93,90}Q_{23}$
1081	0.2	−0.5	$Q_{34,28}Q_{93,90}$
1060	5.3	−0.6	$Q_{75,93}Q_{11,47}$
1025	2.6	1.3	$Q_{93,90}Q_{23}$
1013	4.3	2.0	$Q_{75,72}Q_{22}$
973	13.3	−0.3	$Q_{93,90}Q_{2,26}$
912	8.2	2.9	$Q_{52,39}$
874	13.2	0.4	$Q_{51,27}Q_{93,90}$
773	3.6	0.1	$Q_{90,93,75}Q_{29}$
730	1.5	−2.8	$Q_{75,72}$
710	1.3	1.8	$Q_{93,90,75,72}$
705	2.5	−12.0	$Q_{93,90}$
639	1.2	10.9	$Q_{75,72}$
631	0.7	12.2	$Q_{93,90}$
617	5.7	−1.3	$Q_{93,90,75,72}$
601	1.1	6.8	$Q_{75,73}$
544	0.5	−7.4	$Q_{87,84}$
517	1.6	−15.8	$Q_{68,69}$

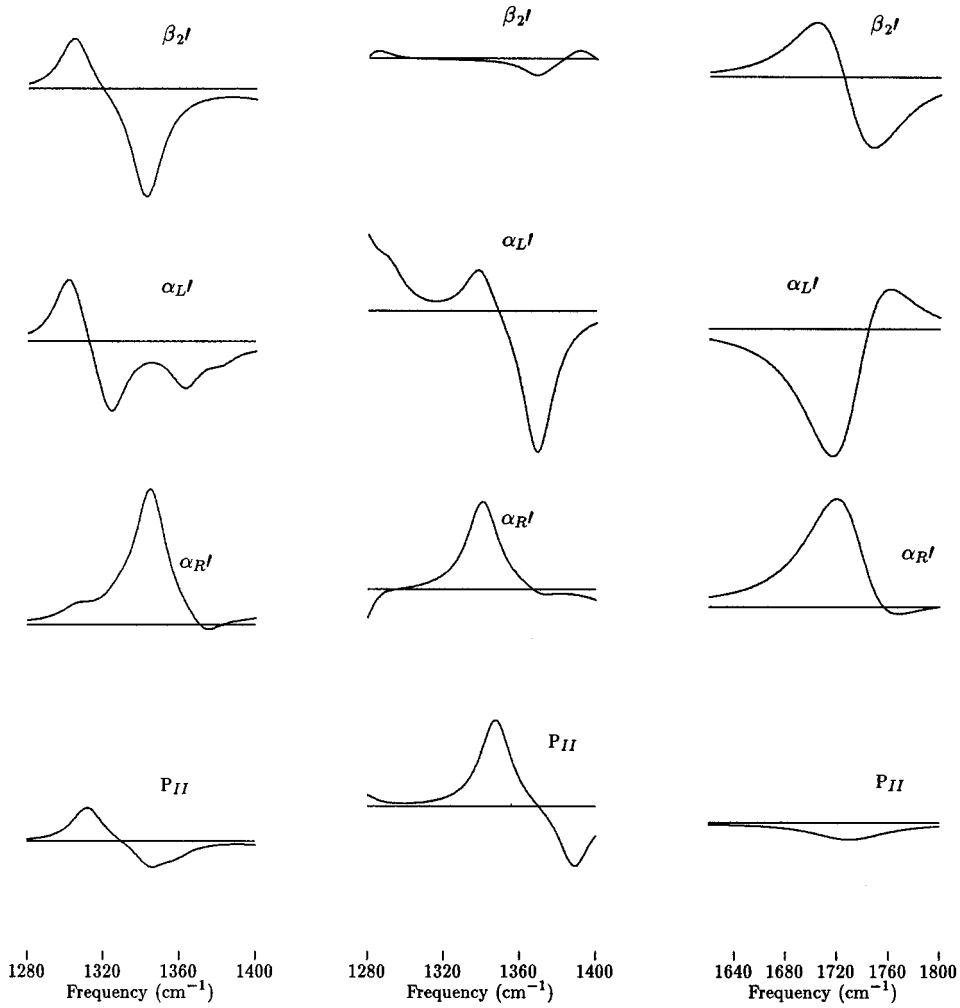

Figure 6. Theoretical VCD spectra. Left: amide III region for the four AAMA+4H_2O conformers. Middle: amide III′ region for the deuterated AAMA+4D_2O conformers. Right: amide I′ region for the deuterated AAMA+4D_2O complexes.

3.2.3. VCD Spectra Analysis. Roberts[10,11] reported the VCD spectra of AAMA in H_2O solution in the amide III region and the deuterated AAMA in D_2O solution in the amide III′ and amide I′ regions, respectively. Our predicted VCD spectra around these regions can be found in Figure 6 for the AAMA+4H_2O (or D_2O) conformers and in Figure 7 for the AAMA+4H_2O (or D_2O)+Onsager conformers. The VCD intensities for the P_{II}+4H_2O+Onsager conformer are given in Table 4. The VCD intensities for the deuterated P_{II}+4D_2O+Onsager conformer are given in Table 5. We now compare our predicted VCD spectral data with the observed spectra in the following subsections.

3.2.3.1. Amide III Region. The observed spectrum of the amide III region (1350−1250 cm^{-1}) shows several weak negative−positive signals for AAMA in H_2O solution. Roberts assigned two modes at 1314 and 1277 cm^{-1} with intensities of +5.6 Δ and −5.6 Δ, respectively.[10] Our predicted amide III modes for the AAMA+4H_2O and the AAMA+4H_2O+Onsager conformers are shown at the left columns in Figures 6 and 7, respectively.

When the bulk solvent is included, the shapes of the VCD spectra in this region do not change much, but the intensities are strengthened. Each of the spectra contains positive and negative modes. If we combine the four spectra together, we may also obtain positive and negative signals. From the modes in this region we cannot say which conformer or what kind of combination of the conformers of AAMA exists in H_2O solution.

3.2.3.2. Amide III′ Region. A single positive signal with an intensity of +7.7 Δ for deuterated AAMA around 1298 cm^{-1} in D_2O solution was reported in ref 10. Our predicted VCD results in the region from 1400 to 1280 cm^{-1} are shown in the middle columns of Figures 6 and 7 for deuterated AAMA+4D_2O and AAMA+4D_2O+Onsager complexes, respectively.

The spectrum of the deuterated α_R' conformer in this region shows one strong positive peak both in model 4 and in model 5. The spectra of deuterated P_{II} and α_L' conformers have two modes with different signs. For the spectra of the deuterated P_{II} conformer, however, the two peaks are relatively far from each other and the positive peak is stronger. From model 4 to model 5, the vibrational mode at 1281 cm^{-1} for the β_2' conformer changed from positive to negative. The modes for the β_2' conformer in this region are very weak. Therefore, the experimentally observed single positive signal may be explained by our predicted spectra of the deuterated α_R' and P_{II} conformers in this region.

3.2.3.3. Amide I′ Region. In ref 10 the spectrum of the amide I′ region (1750−1550 cm^{-1}) of the deuterated AAMA in D_2O solution shows a small negative signal at 1634 cm^{-1} with an intensity of −6.4 Δ. Our predicted VCD results in the region 1800−1620 cm^{-1} are shown in the right columns of Figures 6 and 7 for deuterated AAMA+4D_2O and AAMA+4D_2O+Onsager complexes, respectively.

For the deuterated P_{II}+4D_2O conformer the two amide I′ modes are of nearly the same frequency (1732 and 1731 cm^{-1})

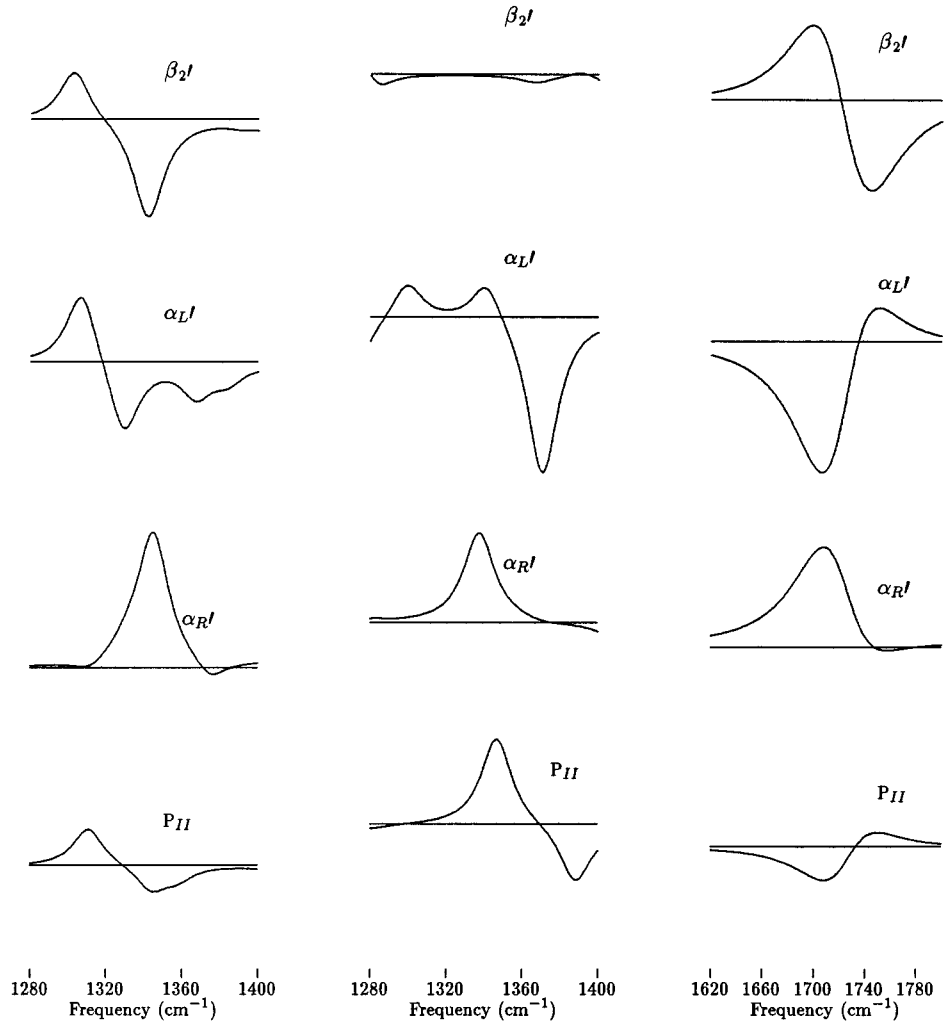

Figure 7. Theoretical VCD spectra. Left: amide III region for the four AAMA+4H_2O+Onsager conformers. Middle: amide III′ region for the deuterated AAMA+4D_2O+Onsager conformers. Right: amide I′ region for the deuterated AAMA+4D_2O+Onsager complexes.

but of positive (98.4 km/mol) and negative (−111.4 km/mol) intensities. One cannot distinguish two modes with such close frequencies; instead one observes only one negative signal, as shown in Figure 6. The VCD calculation for the P_{II}+4D_2O+Onsager conformer shows that these two amide I′ modes have a splitting of 8 cm^{-1} with frequencies 1730 and 1722 cm^{-1} and intensities of 147.1 and −159.9 km/mol, respectively. We see in Figure 7 the negative mode is still stronger than the positive mode. The VCD spectra of other conformers in this region all contain two modes: one positive and one negative with a relatively large splitting (more than 15 cm^{-1}). The α_R' conformer has an obviously stronger mode with a positive intensity, and the α_L' conformer has a similar mode with negative intensity. Here the spectra for the deuterated P_{II} and α_L' conformers may explain the small negative signals observed in the experiment.[10]

As in the case of the Raman spectra, the predicted VCD spectra of the P_{II} conformer are still the best in explaining the experimental observations. Some signals from the α_R' and the α_L' conformers are also consistent with the observed VCD bands.

3.2.4. ROA Spectra Analysis. The ROA spectra calculations have been performed on the four lowest energy AAMA structures within model 5, that is, the P_{II}, α_R', α_L', and β_2' structures. The calculated ROA spectra for P_{II} and deuterated P_{II} are given in Table 6. The ROA spectral simulations for the four conformers and the corresponding deuterated structures are shown in Figure 8 and Figure 9, respectively.

We have extracted the AAMA geometries from the AAMA+4H_2O+Onsager complexes and modified the Hessians and EDEDPD through deleting the components relating to the water coordinates. The EDMDP and the EDEQP were calculated at the 0.005 Å displaced AAMA geometries, and the EDEDPD and the EDEQPD were obtained by finite difference method.

In Figure 8 one sees that none of the four predicted ROA spectra is in perfect agreement with the experimental ROA spectrum, but that the spectrum of the P_{II} structure is in better overall agreement with the observed spectrum than the spectra of the other three structures.

Now we look at the ROA predictions and the signs of the ROA bands for some specific modes, the so-called *amide modes*.

From Figure 8 one can see that two amide I bands in the P_{II} and α_R' conformer spectra have a +/− pattern and the β_2' and α_L' conformer spectra have −/+ patterns. Here our sign pattern identifications are from high to low frequency. In the experimental ROA spectrum we see a small positive peak. The P_{II} spectrum has a positive bias at 1742 cm^{-1} with an intensity of 2.8. This band of P_{II} is consistent with the observed positive peak. The amide I modes of α_R' and β_2' have negative biases, which are inconsistent with the experimental results. The α_L' spectrum in this region has a positive bias, so if only one peak

TABLE 6: ROA Properties ($\Delta \times 10^4$) for P_{II} and Deuterated P_{II} Conformers[a]

P_{II}			P_{II} (d)		
freq	ROA	assign.	freq	ROA	assign.
1742	2.8	$Q_{3,13,22,1}$	1733	1.4	$Q_{13,3,12,1}$
1731	−1.5	$Q_{13,3,12}$	1725	3.5	$Q_{3,13,12,1}$
1643	−10.5	$Q_{23,12}$	1539	−29.9	$Q_{41,10,36}$
1637	3.7	$Q_{22,1}$	1534	17.6	$Q_{36,41,37}$
1536	7.8	$Q_{41,43}$	1526	4.9	$Q_{41,10,36}$
1530	−6.0	$Q_{36,37,38}$	1524	1.7	$Q_{37,36}$
1524	6.0	$Q_{37,36,39}$	1516	−6.4	$Q_{32,34}$
1519	−20.1	$Q_{31,32,33}$	1514	8.0	$Q_{42,12,36}$
1515	−0.7	$Q_{32,31,34}$	1510	1.0	$Q_{42,12}$
1511	−1.9	$Q_{42,44}$	1479	−35.5	$Q_{1,31,22}$
1476	8.5	Q_{40}	1466	−6.1	$Q_{40,17,12}$
1441	−2.7	$Q_{35,45}$	1434	−20.7	Q_{35}
1433	15.3	$Q_{30,2}$	1430	6.7	Q_{30}
1424	11.7	$Q_{35,46,45}$	1388	1.4	$Q_{45,46}$
1358	5.9	$Q_{45,1,46}$	1346	−2.1	$Q_{46,45}$
1344	−16.9	$Q_{45,1,22}$	1203	4.2	Q_{43}
1311	1.8	$Q_{46,12,23}$	1192	−1.1	$Q_{39,4,48}$
1203	2.4	Q_{43}	1177	23.0	$Q_{22,4}$
1197	−6.6	$Q_{4,39,48}$	1160	1.5	Q_{44}
1163	−1.4	$Q_{44,42}$	1111	3.6	$Q_{38,33}$
1132	1.9	$Q_{11,38,4}$	1089	−1.6	$Q_{23,17,12}$
1086	22.5	$Q_{38,34,33}$	1081	−2.7	$Q_{34,28}$
1079	−15.3	$Q_{34,28}$	1060	−13.9	$Q_{11,4}$
1064	−9.4	Q_{17}	1025	−0.4	$Q_{17,23}$
1045	5.3	$Q_{33,11}$	1012	−6.2	$Q_{33,22}$
982	−1.4	$Q_{2,11}$	973	1.9	$Q_{2,11}$
925	3.6	$Q_{39,52,4}$	912	3.2	$Q_{39,4}$
883	0.1	$Q_{9,51,43}$	874	0.5	$Q_{9,51,43}$
875	18.6	$Q_{59,25}$	773	−11.2	$Q_{29,47}$
869	−20.5	$Q_{55,56,24}$	709	−3.7	$Q_{27,47,49}$
767	2.3	$Q_{29,47,25}$	642	15.8	$Q_{55,56,28}$
712	−0.1	$Q_{27,47,49}$	626	23.2	$Q_{59,25}$
621	0.1	$Q_{26,2}$	615	−3.1	$Q_{26,2,25}$
611	14.7	$Q_{28,34}$	600	18.2	$Q_{28,24,34}$
522	−0.9	$Q_{50,48,51}$	514	−0.9	$Q_{50,48,51}$
405	−5.4	$Q_{26,50,29}$	404	−5.4	$Q_{26,50,29}$
358	−3.3	$Q_{48,53,50}$	355	−2.8	$Q_{53,48}$
336	−20.8	$Q_{27,47,53}$	333	−17.8	$Q_{47,27}$
276	12.6	$Q_{57,53,51}$	274	13.5	$Q_{57,53,51}$
265	3.7	$Q_{49,25,48}$	264	2.9	$Q_{49,48}$
234	14.4	$Q_{57,51}$	233	14.2	$Q_{57,51}$
186	9.2	$Q_{52,48,58}$	185	9.7	$Q_{52,48}$
169	3.4	$Q_{25,58}$	168	2.9	$Q_{25,58}$
132	39.0	Q_{54}	132	37.9	Q_{54}
110	6.2	$Q_{58,59,56}$	109	6.4	$Q_{58,56}$
97	−3.2	$Q_{58,55,54}$	96	−3.2	$Q_{58,55,54}$
71	−8.0	$Q_{60,44}$	70	−8.1	$Q_{60,44}$
57	1.8	$Q_{56,58}$	57	1.8	$Q_{56,58}$

[a] Only the AAMA geometries were taken from the corresponding AAMA+4H_2O structures optimized in the Onsager solvent model. Hessians and electric dipole−electric dipole polarizability derivatives were also taken from the corresponding results for the AAMA+4H_2O+Onsager calculations through deleting the portions relating to the H_2O coordinates. RHF/6-31G* electric dipole−electric quadrupole and electric dipole−magnetic dipole polarizabilities were calculated on these AAMA geometries to get the ROA spectra.

is resolvable, then this spectrum is also in agreement with the experimentally observed positive peak.

Next we look at the amide I′ bands for the D_2O solution spectra (Figure 9). The experimental ROA spectrum seems to have two positive peaks, but as the signal to noise is quite low, one cannot be sure. Note that Deng and co-workers predict a +/− pattern for the amide I′ peaks for their P_{II} conformer while our calculations for the P_{II} conformer predict two positive peaks, which is consistent with the experimentally observed positive band(s). This better agreement may be due to the influence of waters. Note that their structure was actually a transition state for the isolated state of AAMA, while ours is in the same region

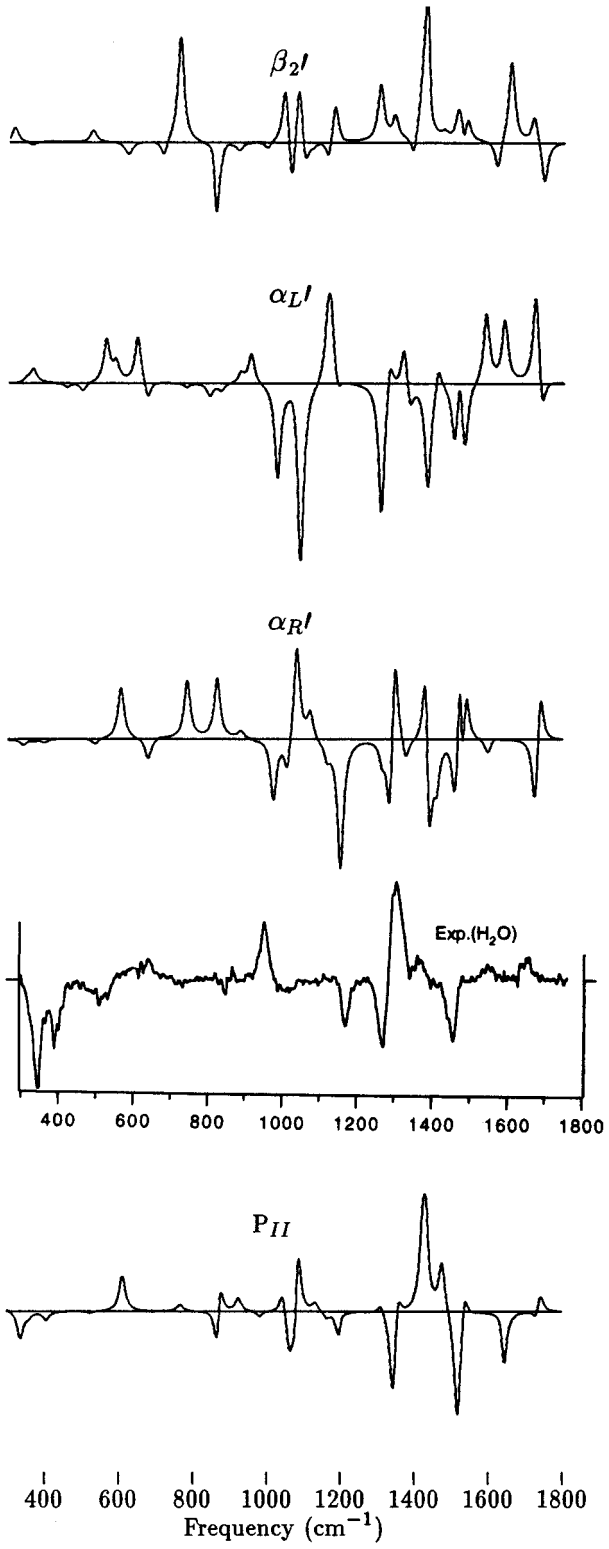

Figure 8. Experimental ROA spectrum of AAMA in H_2O (from ref 13) and calculated ROA spectra for the four AAMA structures obtained from the AAMA+4H_2O+Onsager complexes.

but now a minimum. The spectra of the α_L' and the α_R' conformers also have positive biases. Only the amide I′ modes of the β_2' conformer have negative bias and are inconsistent with the observed positive band(s). The spectrum for the P_{II} conformer in this region is the best in agreement with the observed ROA spectra.

In Figure 8, in the region from 1600 cm^{-1} to approximately 1100 cm^{-1} we predict strong bands with a sign pattern of −/− /+/+/−/− for the P_{II} conformer. The experimental ROA

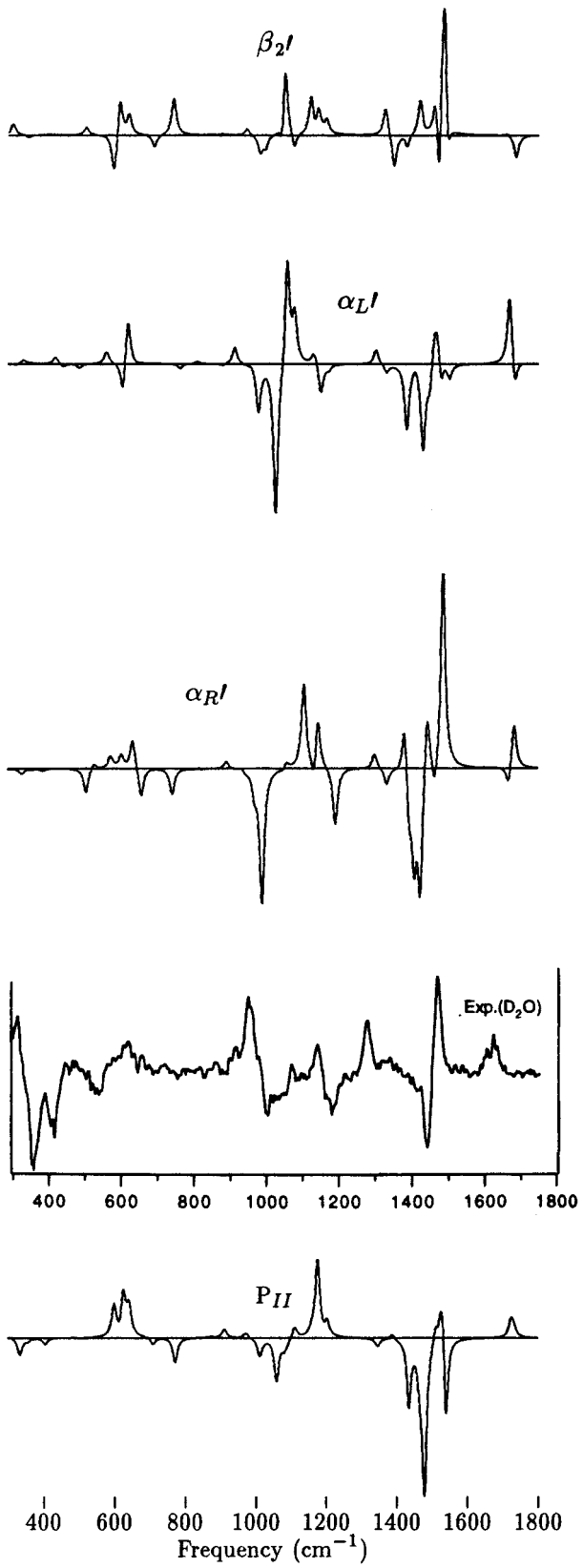

Figure 9. Experimental ROA spectrum of AAMA in D_2O (from ref 13) and calculated ROA spectra for the four deuterated AAMA structures obtained from the AAMA+4D_2O+Onsager complexes.

spectrum in this region has a sign pattern of +/−/+/+/−/−, agreeing well with that for the P_{II} conformer, except for the first band with the wrong sign. None of the other three predicted ROA spectra are in good agreement with the experimental ROA spectrum.

In the region from 1100 to 500 cm^{-1} the predicted ROA spectra for none of the four conformers are in good agreement with the observed ROA spectrum.

In the region from 500 to 300 cm^{-1} the predicted ROA spectra for P_{II} and α_R' conformers both predict two negative bands, which is in agreement with the experimental ROA spectrum in this region. The predicted ROA spectra for the β_2' and α_L' conformers both have positive bands, which is inconsistent with the observed spectrum. The two negative bands predicted for the P_{II} conformer have larger intensities than for the α_R' conformer. Since the experimental ROA spectrum has two large negative peaks, it is possible that both the P_{II} andα_R' conformers are present in aqueous solution.

Now look at the ROA spectra of AAMA in D_2O solution (Figure 9). In the region from 1600 to 1100 cm^{-1} the experimental ROA spectrum has strong bands with a sign pattern of +/−/+/−/+. The predicted ROA spectrum of the P_{II} conformer has a sign pattern of −/−/−/+/−, and the predicted spectrum of the α_R' conformer has a sign pattern of +/−/+/−/+. Therefore the spectrum for α_R' is in much better agreement with the experimentally observed sign pattern in this region than the P_{II} conformer. In this region the predicted sign patterns of the ROA spectra for β_2' and α_L' are not in good agreement with the experimental observation.

In the region from 500 to 300 cm^{-1} the experimental ROA spectrum for AAMA in D_2O solution has two negative bands, which is consistent with the predicted ROA spectra for both the P_{II} and α_R' conformers. The predicted ROA spectra for the β_2' and α_L' conformers have positive features which are not in agreement with the experimentally observed features.

4. Conclusions

To simulate the spectra (VA, Raman, VCD, and ROA) of AAMA in aqueous solutions, we have solvated the AAMA with four explicit water molecules. For including the bulk effect of water, we then put the explicitly solvated AAMA conformers into the self-consistent reaction field Onsager model with a dielectric constant of $\epsilon = 80.0$. Eight AAMA conformers have been considered. For four of them (i.e., β_2', α_L', α_R', and P_{II} with 4H_2O), we have calculated the VA, Raman, and VCD spectra. Taking only the AAMA geometries from the four complexes, we have performed the ROA spectra calculations.

Our work shows that the explicit water molecules play an important role in stabilizing conformations of AAMA that may not be stable in the isolated state. The normal modes of AAMA and its surrounding waters are vibrationally coupled. The interactions between the waters and the AAMA will strongly influence the VA and VCD spectra of AAMA. The continuum solvent model may further modify the orientations of the explicit water molecules and the structure of AAMA, thereby making corrections to the vibrational frequencies and intensities.

From the comparison and analysis of the Raman, VCD, and ROA spectra of the β_2', α_L', α_R', and P_{II} conformers, we found that the spectra of the P_{II} structure are the best to explain most of the experimental Raman, VCD, and ROA spectra of AAMA in H_2O and in D_2O solutions. Some of the Raman, VCD, and many ROA bands of α_R' can also fit the experimental signals. Deng et al.[13] reported that a majority of the observed ROA bands of the AAMA in H_2O solution are found to have corresponding bands in the spectra predicted for their P_{II} conformer ($\phi = -99°$, $\psi = 136°$). Some other simulations or free energy calculations suggest that the P_{II} conformers of the AAMA ($\phi = -110°$ to $-70°$, $\psi = 120°$ to 150°) have relatively lower free energies in H_2O solution.[7,8,18,20,21] On the other hand, the α_R region of the conformational space was also found to be significantly

stabilized due to polarization effects.[8,18,20−22] Therefore, the P_{II} structure may really play an important role for AAMA in aqueous solution. The conformers around α'_R can also exist. The predicted Raman, VCD, and ROA spectra of α'_L are not as good as those of P_{II} and α'_R. Since the experiments are normally taken at room temperature and our spectral calculations do not take into account temperature effects, α'_L and some other conformers of AAMA can also be present in H_2O solutions.

This work again shows the capabilities of explicitly adding water to DFT calculations and simulating the Raman and VCD spectra of small peptides in solution. The solvation effect has been shown to have a significant influence on the Raman, VCD, and ROA spectra.[10,11,13] By adding explicit water molecules and the Onsager continuum model, we have included both the effects of the H-bonding and the bulk water. After optimizing the geometry and calculating the Hessian and APT we need to calculate additional tensors to predict the VCD, Raman, and ROA spectra. These tensor derivatives have not all been implemented at the DFT level of theory within the continuum models. Hence we have calculated the AAT, EDEDPD, EDMDPD, and EDEQPD all at the RHF of theory with split valence plus basis sets. The AAT and EDEDPD were calculated with the waters present, while the finite difference EDMDPD and EDEQPD were calculated only for AAMA. As these calculations are quite expensive and adding the waters would greatly increase the cost, we have settled for this compromise in this work. Note that this is the level of theory that has been used by all other groups to date and has been shown to predict the ROA spectra quite well. We realize that the effect of the waters may be important in the EDMDPD and EDEQPD calculations; we are pursuing this problem on a simpler system.[57]

We hope that these calculations will motivate further experimental VCD and ROA experiments on AAMA and other calculations on other peptide models using explicit water molecules. We have performed calculations only on AAMA, and this methodology needs to be applied to other systems. We are also following these lines on two other model systems in our laboratories: the structures of L-alanine and L-alanyl-L-alanine in aqueous solution. As both of these molecules are zwitterions in aqueous solution, they present special problems. We look forward to presenting our results in future publications.

Acknowledgment. We would like to thank Dr. Nicholas Handy and Dr. Roger Amos for providing us a copy of CADPAC 5.2 used for the tensors calculations. The generous support of computer time on the IBM/SP2 of the German Cancer Research Center and on the SGI Power Challenge Denmark in Lyngby is also greatefully acknowledged. We are indebted to Michaela Knapp-Mohammady for technical assistance in preparing the manuscript.

References and Notes

(1) Jalkanen, K. J.; Suhai, S. *Chem. Phys.* **1996**, *208*, 81.
(2) Grenie, Y.; Avignon, M.; Garrigou-Lagrange, C. *J. Mol. Struct.* **1975**, *24*, 293.
(3) Head-Gordon, T.; Head-Gordon, M.; Frisch, M. J.; Brooks, C. L., III; Pople, J. A. *J. Am. Chem. Soc.* **1991**, *113*, 5989.
(4) Böhm, H.-J.; Brode, S. *J. Am. Chem. Soc.* **1991**, *113*, 7129.
(5) Frey, R. F.; Coffin, J.; Newton, S. Q.; Ramek, M.; Cheng, V. K. W.; Momany, F. A.; Schäfer, L. *J. Chem. Soc.* **1992**, *114*, 5369.
(6) Gould, I. R.; Kollman, P. A. *J. Phys. Chem.* **1992**, *96*, 9255.
(7) Tobias, D. J.; Brooks, C. L., III. *J. Chem. Phys.* **1992**, *96*, 3864.
(8) Brooks, C. L., III; Cases, D. A. *Chem. Rev.* **1993**, *93*, 2487.
(9) Gould, I. R.; Cornell, W. D.; Hillier, I. H. *J. Am. Chem. Soc.* **1994**, *116*, 9250.
(10) Roberts, G.-M. L. Vibrational Circular Dichroism and Normal Coordinate Analysis of Alanine Dipeptides and Several Deuterared Isotopomers. Ph.D. Thesis, The City University of New York, 1990.
(11) Roberts, G.-M. L.; Diem, M. *Proceedings of the Second European Conference Spectroscopy of Biological Molecules*: Wiley: Freiburg, Germany, 1987; p 77.
(12) Avignon, M.; Garrigou-Lagrange, C. *Biopolymers* **1973**, *12*, 1651.
(13) Deng, Z.; Polavarapu, P. L.; Ford, S. J.; Hecht, L.; Barron, L. D.; Ewig, C. S.; Jalkanen, K. J. *J. Phys. Chem.* **1996**, *100*, 2025.
(14) Tomasi, J.; Persico, M. *Chem. Rev.* **1994**, *94*, 2027.
(15) Chen, X. G.; Schweitzer-Stenner, S.; Krimm, S.; Mirkim, N. G.; Asher, S. A. *J. Am. Chem. Soc.* **1994**, *116*, 11141.
(16) Sieler, G.; Schweitzer-Stenner, R. *J. Am. Chem. Soc.* **1997**, *119*, 1720.
(17) Pettitt, B. M.; Karplus, M. J. *J. Phys. Chem.* **1988**, *92*, 3994.
(18) Madison, V.; Kopple, K. D. *J. Am. Chem. Soc.* **1980**, *102*, 4855.
(19) Mezei, M.; Mehrotra, P. K.; Beveridge, D. L. *J. Am. Chem. Soc.* **1985**, *107*, 2239.
(20) Anderson, A. G.; Hermans, J. *Proteins: Struct. Funct. Genet.* **1988**, *3*, 262.
(21) Schmidt, A. B.; Fine, R. M. *Mol. Simul.* **1994**, *13*, 347.
(22) Ösapay, K.; Young, W. S.; Bashford, D.; Brooks, C. L., III; Case, D. A. *J. Phys. Chem.* **1996**, *100*, 2698.
(23) Gilson, M. K.; McCammon, J. A.; Madura, J. D. *J. Comput. Chem.* **1995**, *16*, 1081.
(24) Han, W.-G.; Suhai, S. *J. Phys. Chem.* **1996**, *100*, 3942.
(25) Parr, R. G.; Yang, W. *Density-Functional Theory of Atoms and Molecules*; Oxford University Press: New York, 1989.
(26) Labanowski, J. K.; Andzelm, J., Eds. *Density Functional Methods in Chemistry*; Springer-Verlag: New York, 1991.
(27) Frisch, M. J.; Trucks, G. W.; Schlegel, H. B.; Gill, P. M. W.; Johnson, B. G.; Robb, M. A.; Cheeseman, J. R.; Keith, T. A.; Petersson, G. A.; Montgomery, J. A.; Raghavachari, K.; Al-Laham, M. A.; Zakrzewski, V. G.; Ortiz, J. V.; Foresman, J. B.; Cioslowski, J.; Stefanov, B. B.; Nanayakkara, A.; Challacombe, M.; Peng, C. Y.; Ayala, P. Y.; Chen, W.; Wong, M. W.; Andres, J. L.; Replole, E. S.; Gomperts, R.; Martin, R. L.; Fox, D. J.; Binkley, J. S.; Defrees, D. J.; Baker, J.; Stewart, J. J. P.; Head-Gordon, M.; Gonzalez, C.; Pople, J. A. *Gaussian 94 User's Guide*; Gaussian Inc.: Pittsburgh, PA, 1994.
(28) Becke, A. D. J. *J. Chem. Phys.* **1992**, *96*, 2155.
(29) Becke, A. D. J. *J. Chem. Phys.* **1992**, *97*, 9173.
(30) Becke, A. D. J. *J. Chem. Phys.* **1993**, *98*, 5648.
(31) Lee, C.; Yang, W.; Parr, R. G. *Phys. Rev. B* **1988**, *37*, 785.
(32) *Insight II User Guide*; San Diego, CA, 1995.
(33) Beglov, D.; Roux, B. *Biopolymers* **1995**, *35*, 171.
(34) Amos, R. D.; Alberts, I. L.; Andrews, J. S.; Colwell, S. M.; Handy, N. C.; Jayatilaka, D.; Knowles, P. J.; Kobayashi, R.; Koga, N.; Laidig, K. E.; Maslen, P. E.; Murray, C. W.; Rice, J. E.; Sanz, J.; Simandiras, E. D.; Stone, A. J.; Su, M.-D. *Cambridge Analytical Derivatives Package (CADPAC)*, 5.2 ed.; Cambridge: U.K., 1994.
(35) Amos, R. D. *Chem. Phys. Lett.* **1982**, *87*, 23.
(36) Helgaker, T.; Rund, K.; Bak, K. L.; Jourgensen, P.; Olsen, J. *Faraday Discuss.* **1994**, *99*, 165.
(37) Polavarapu, P. L. *J. Phys. Chem.* **1990**, *94*, 8106.
(38) Amos, R. D. *Chem. Phys. Lett.* **1986**, *124*, 376.
(39) Frisch, M. J.; Yamaguchi, Y.; Gaw, J. F.; Schaefer, H. F., III; Binkley, J. S. *J. Chem. Phys.* **1986**, *84*, 531.
(40) Diem, M. *Introduction to Modern Vibrational Spectroscopy*; John Wiley & Sons: New York, 1993.
(41) Barron, L. D.; Buckingham, A. D. *Mol. Phys.* **1971**, *20*, 1111.
(42) Barron L. D. *Molecular Light Scattering and Optical Activity*; Cambridge University Press: Cambridge, U.K., 1982.
(43) Buckingham, A. D. *Adv. Chem. Phys.* **1971**, *12*, 107.
(44) Hecht, L.; Barron, L. D. *Appl. Spectrosc.* **1990**, *44*, 483.
(45) Barron, L. D.; Ford, S. J.; Bell, A. F.; Wilson, G.; Hecht, L.; Cooper, A. *Faraday Discuss.* **1994**, *99*, 217.
(46) Cheam, T. C. *J. Mol. Struct.* **1993**, *295*, 259.
(47) Mirkin, N. G.; Krimm, S. *J. Am. Chem. Soc.* **1991**, *113*, 9742.
(48) Mirkim, N. G.; Krimm, S. *J. Mol. Struct.* **1996**, *377*, 219.
(49) Williams R. W. *Biopolymers* **1992**, *32*, 829.
(50) (a) Jalkanen, K. J.; Stephens, P. J. *J. Phys. Chem.* **1991**, *95*, 5446. (b) Jalkanen, K. J. Ph.D Thesis, University of Southern California, 1989.
(51) Finley, J. W.; Stephens, P. J. *J. Mol. Struct. (THEOCHEM)* **1995**, *357*, 225.
(52) Stephens, P. J.; Devlin, F. J.; Ashvar, C. S.; Chabalowski, C. F.; Frisch, M. J. *Faraday Discuss.* **1994**, *99*, 103.
(53) Devlin, F. J.; Stephens, P. J.; Cheeseman, J. R.; Frisch, M. J. *J. Am. Chem. Soc.* **1996**, *118*, 6327.
(54) Stephens, P. J.; Devlin, F. J.; Chabalowski, C. F.; Frisch, M. J. *J. Phys. Chem.* **1994**, *98*, 11623.
(55) El-Azhary, A. A.; Suter, H. U. *J. Phys. Chem.* **1996**, *100*, 15056.
(56) Bour, P.; Tam, C. N.; Shaharuzzaman, M.; Chickos, J. S.; Keiderling, T. A. *J. Phys. Chem.* **1996**, *100*, 15041.
(57) Jalkanen, K. J.; Suhai, S. To be published.